Catalytic activity of the Bin3/MEPCE methyltransferase domain is dispensable for 7SK snRNP function in *Drosophila melanogaster*

Ryan J Palumbo, Steven D Hanes

Department of Biochemistry & Molecular Biology, SUNY Upstate Medical University

750 East Adams Street, 4283 Weiskotten Hall, Syracuse, New York, 13210

PalumboR@upstate.edu, HanesS@upstate.edu

Unexpected *in vivo* results with Bin3

Keywords: Bin3, Bmc1, Bcdin3, MEPCE, Mepcea, 7SK, P-TEFb, RNA Polymerase II, Promoter-Proximal Pausing, Transcription Elongation

ABSTRACT

Methylphosphate Capping Enzyme (MEPCE) monomethylates the gamma phosphate at the 5′ end of the 7SK noncoding RNA, a modification thought to protect 7SK from degradation. 7SK serves as a scaffold for assembly of a snRNP complex that inhibits transcription by sequestering the positive elongation factor P-TEFb. While much is known about the biochemical activity of MEPCE *in vitro*, little is known about its functions *in vivo*, or what roles— if any—there are for regions outside the conserved methyltransferase domain. Here, we investigated the role of Bin3, the *Drosophila* ortholog of MEPCE, and its conserved functional domains in *Drosophila* development. We found that *bin3* mutant females had strongly reduced rates of egg-laying, which was rescued by genetic reduction of P-TEFb activity, suggesting that Bin3 promotes fecundity by repressing P-TEFb. *bin3* mutants also exhibited neuromuscular defects, analogous to a patient with *MEPCE* haploinsufficiency. These defects were also rescued by genetic reduction of P-TEFb activity, suggesting that Bin3 and MEPCE have conserved roles in promoting neuromuscular function by repressing P-TEFb. Unexpectedly, we found that a Bin3 catalytic mutant (Bin3^{Y795A}) could still bind and stabilize 7SK and rescue all *bin3* mutant phenotypes, indicating that Bin3 catalytic activity is dispensable for 7SK stability and snRNP function *in vivo*. Finally, we identified a metazoan-specific motif (MSM) outside of the methyltransferase domain and generated mutant flies lacking this motif (Bin3$^{\Delta MSM}$). Bin3$^{\Delta MSM}$ mutant flies exhibited some—but not all—*bin3* mutant phenotypes, suggesting that the MSM is required for a 7SK-independent, tissue-specific function of Bin3.

INTRODUCTION

Regulation of eukaryotic RNA polymerase II (RNAPII) occurs at multiple stages of the transcription cycle, including RNAPII recruitment to promoters by enhancer binding proteins, the establishment of the pre-initiation complex, and promoter release. In higher eukaryotes an additional mechanism, promoter-proximal pausing, has been shown to be critical for RNAPII regulation in development and in response to signaling events (Margaritis and Holstege 2008; Gilmour 2009; Chiba *et al.* 2010; Levine 2011; Li and Gilmour 2011; Nechaev and Adelman 2011; Adelman and Lis 2012; Zhou *et al.* 2012; Gaertner and Zeitlinger 2014; Jonkers and Lis 2015; Liu *et al.* 2015; Mayer *et al.* 2017; Chen *et al.* 2018; Core and Adelman 2019; Dollinger and Gilmour 2021; Gonzalez *et al.* 2021; Abuhashem *et al.* 2022). Pausing occurs when RNAPII stalls after transcribing approximately 30-60 nucleotides, and is induced by the binding of negative elongation factors (Yamaguchi *et al.* 1999; Wang *et al.* 2010) and by hypo-phosphorylation of serine 2 (Ser2) in the heptad repeat (YSPTSPS) of the carboxy-terminal domain of the large subunit of RNAPII (reviewed in Brookes and Pombo 2009). Promoter proximal pausing is relieved by the kinase activity of Positive Transcription Elongation Factor b (P-TEFb; Marshall and Price 1995), which is a heterodimer composed of Cyclin-dependent kinase 9 (Cdk9; Marshall *et al.* 1996) and the regulatory cyclin, Cyclin T (CycT; Peng *et al.* 1998). P-TEFb phosphorylates negative elongation factors (Wada *et al.* 1998; Cheng and Price 2007) and Ser2 (Zhou *et al.* 2000; Ramanathan *et al.* 2001; Shim *et al.* 2002; Ni *et al.* 2004), which allows RNAPII to enter productive elongation (Ni *et al.* 2008).

To maintain a balance between transcription elongation and pausing, P-TEFb activity is highly regulated; without this regulation, P-TEFb becomes "hyper-activated" and induces aberrant transcription elongation (Schneeberger *et al.* 2019). Key to this regulation is the 7SK snRNP, which sequesters (and thereby represses) P-TEFb (Nguyen *et al.* 2001; Yang *et al.* 2001). The "core" 7SK snRNP is composed of the 7SK noncoding RNA, which acts as a scaffold for the proteins

Methylphosphate Capping Enzyme (MEPCE) and La-Related Protein 7 (LARP7) (Krueger *et al.* 2008; Barboric *et al.* 2009; Xue *et al.* 2010; Muniz *et al.* 2013; Brogie and Price 2017; Yang *et al.* 2022). MEPCE and LARP7 protect the 5′ and 3′ ends of 7SK from exoribonucleolytic degradation, respectively (Jeronimo *et al.* 2007; Markert *et al.* 2008; Barboric *et al.* 2009; Xue *et al.* 2010; Muniz *et al.* 2013). After formation of the core snRNP, 7SK RNA is reversibly bound by a homodimer of Hexamethylene Bis-Acetamide Inducible Protein (HEXIM) (Blazek *et al.* 2005; Li *et al.* 2005). Binding of HEXIM to 7SK induces a conformational change that allows HEXIM to bind to P-TEFb (Michels *et al.* 2004), functionally sequestering and inactivating P-TEFb (Yik *et al.* 2004). Upon cellular stress and other cellular signals (reviewed in Liu *et al.* 2015), binding of accessory proteins to 7SK (Herreweghe *et al.* 2007; Barrandon *et al.* 2007; Krueger *et al.* 2008; Lemieux *et al.* 2015; Bugai *et al.* 2019) and a concomitant conformational change in the secondary structure of 7SK RNA (Krueger *et al.* 2010; Yang *et al.* 2022) releases P-TEFb from the repressive 7SK snRNP. P-TEFb is then able to relieve pausing to enable transcription elongation.

MEPCE is the long sought-after RNA methyltransferase that uses the methyl donor S-adenosyl-methionine (SAM) to add a monomethyl cap to the gamma phosphate on the 5′ end of 7SK (Gupta *et al.* 1990a; Shumyatsky *et al.* 1990; Shimba and Reddy 1994), an RNA polymerase III transcript (Zieve and Penman 1976; Murphy *et al.* 1986, 1987, 1989; Shumyatsky *et al.* 1990). MEPCE is human ortholog of Bin3, a *Drosophila* protein that is the founding member of the Bin3/MEPCE/Bmc1 family of RNA methyltransferases (Zhu and Hanes 2000; Jeronimo *et al.* 2007; Barboric *et al.* 2009; Cosgrove *et al.* 2012; Páez-Moscoso *et al.* 2022; Porat *et al.* 2022). We originally discovered Bin3 as an interacting partner of the Bicoid homeodomain protein (Zhu and Hanes 2000). Bicoid acts as both an activator of zygotic gene transcription, and a translational repressor of maternal *caudal* mRNA during embryogenesis; both functions are critical for anterior-posterior patterning (Dubnau and Struhl 1996; Rivera-Pomar *et al.* 1996; Chan and Struhl 1997; Niessing *et al.* 1999, 2000, 2002; Cho *et al.* 2005). We

had hypothesized that Bin3 was an arginine methyltransferase that methylated Bicoid to alter its function, transitioning Bicoid from being a transcriptional activator to a translational repressor, or vice versa. However, identification and characterization of MEPCE in human cells (originally called BCDIN3) demonstrated that it is actually an RNA methyltransferase that targets 7SK to form a snRNP that represses transcription (Jeronimo *et al.* 2007). We later showed that early in *Drosophila* embryogenesis, Bin3 stabilizes 7SK to form a novel snRNP containing Bin3 and Bicoid (and potentially other translational factors) that represses translation of maternal *caudal* mRNA at the anterior of the embryo (Singh *et al.* 2011). It is important to note that Bicoid is an insect-specific protein, and therefore, the translational repression function of Bin3 is also likely to be insect-specific. The canonical role of Bin3/MEPCE in regulating transcription elongation, and the importance of this regulation to normal development, has not been extensively studied in *Drosophila* or in other model organisms (see below).

Much of what we know about the 7SK RNA binding and capping functions of MEPCE comes from *in vitro* or cell culture-based studies focusing on the methyltransferase activity of MEPCE and the stepwise assembly of the 7SK snRNP. The monomethyl cap is believed to protect the 5′ end of 7SK from exoribonucleolytic degradation (Shumyatsky *et al.* 1993). However, MEPCE is peculiar in that unlike most enzymes, it remains bound to the product of the reaction it catalyzes, calling into question the essentiality of methyl capping. MEPCE that is constitutively bound to capped 7SK facilitates the stable binding of LARP7 (Xue *et al.* 2010) to form the core 7SK snRNP (Muniz *et al.* 2013). Several residues in the active site have been identified as being essential for binding to SAM and/or 7SK (Xue *et al.* 2010; Shelton *et al.* 2018), and for methyltransferase activity (Yang *et al.* 2019). Pre-association of MEPCE with 7SK was found to enhance the recruitment of LARP7 to 7SK and to MEPCE itself (Xue *et al.* 2010). However, whether methyltransferase activity is required *in vivo* for 7SK binding and stability, and 7SK snRNP function, has never explicitly been tested. Moreover, these studies have focused primarily on the function of the methyltransferase domain. During evolution, MEPCE orthologs have acquired extensive

protein sequence flanking the methyltransferase domain, the conservation and function(s) of which have not been explored.

Underscoring the need to understand the function of MEPCE *in vivo*, there is a neurodevelopmental disorder that is caused by heterozygosity for a nonsense mutation in *MEPCE* that results in P-TEFb hyper-activation (Schneeberger *et al.* 2019). However, our ability to study the *in vivo* function of MEPCE and its orthologs is limited by the fact that MEPCE function appears to be essential in vertebrate model organisms. For example, transfecting HeLa cells with siRNAs to destabilize 7SK (which phenocopies the destabilization of 7SK in the absence of MEPCE function) results in apoptosis (Haaland *et al.* 2005); treating zebrafish embryos with morpholino oligonucleotides targeting *mepcea* (the zebrafish ortholog of *MEPCE*; originally named *bcdin3*) is embryonic lethal (Barboric *et al.* 2009), precluding the ability to study Mepcea function in adult zebrafish; and deleting 7SK in mice (which also phenocopies the destabilization of 7SK in the absence of MEPCE function) is lethal (Xu *et al.* 2022), precluding the ability to study MEPCE function in adult mice. However, deleting *bin3* (the *Drosophila* ortholog of *MEPCE*) does not affect the viability of adult *Drosophila* (Singh *et al.* 2011). Therefore, *Drosophila* Bin3 provides a model to study the *in vivo* functions of MEPCE in metazoan development.

Here, we investigated the role of Bin3 in *Drosophila* development. We found that Bin3 is required for fecundity and has a conserved role in promoting neuromuscular function, by repressing P-TEFb. Unexpectedly, we found that Bin3 catalytic activity is dispensable for 7SK stability and snRNP function *in vivo*, challenging the paradigm that methyl capping is essential for 7SK stability. Finally, we identified a metazoan-specific motif (MSM) outside of the methyltransferase domain that confers a 7SK-independent, tissue-specific function to Bin3. These studies illustrate the importance of establishing a model system in which to study this important and conserved enzyme.

127 **MATERIALS AND METHODS**

128 **Fly stocks and husbandry**

129 Fly stocks from the Bloomington *Drosophila* Stock Center (BDSC) used in this study are listed in
130 **Table S1**. Fly stocks we constructed for this study are listed in **Table S2**. The genotypes of maternal and
131 paternal flies, and the genotypes of their progeny used for experiments, and the figures in which those
132 experiments appear, are listed in **Table S3**. Fly were reared at 25°C and 60-80% humidity on a 12-hour
133 light/dark cycle, on either Nutri-Fly MF food (Genesee Scientific) with ~0.064 M propionic acid (Sigma
134 Aldrich, P5561; or Apex Bioresearch Products, 20-271), or food made based on the Nutri-Fly MF
135 formula: 25 g/L Inactive Dry Yeast (Genesee Scientific), 89.5 g/L Dry Molasses (Genesee Scientific), 57
136 g/L Fly Stuff Yellow Cornmeal (Genesee Scientific), 5.84 g/L Nutri-Fly *Drosophila* Agar, Gelidium
137 (Genesee Scientific), ~0.064 M propionic acid (Apex Bioresearch Products).

138

139 ***bin3* mutants**

140 We previously described two excision alleles that remove some ($bin3^{4-7}$) or all ($bin3^{2-7}$) of the *bin3*
141 coding exons (Parks *et al.* 2004; Singh *et al.* 2011). Both alleles were made in the same background, and
142 when placed in *trans* to produce $bin3^{4-7}/bin3^{2-7}$ mutants, incurred background effects likely due to
143 homozygosity for recessive second-site mutations. To produce *bin3* mutants that avoid these
144 confounding effects, we crossed flies heterozygous for $bin3^{2-7}$ (**Fig. 1a**) with flies heterozygous for a
145 deficiency uncovering *bin3* (*Df*, **Fig. 1a**), which is in a different genetic background than $bin3^{2-7}$ (Ryder *et*
146 *al.* 2004).

147

148 **Generation of transgenic $bin3^{+}$ rescue flies**

149 We previously showed that Bin3 is required for embryonic viability by demonstrating a *bin3* cDNA under
150 control of the maternal *Hsp83* promoter rescued the embryonic lethality of eggs laid by *bin3* mutant

151 females (Singh *et al.* 2011). To examine the role of Bin3 more broadly, we needed a rescue approach
152 that would faithfully express *bin3* under control of its own regulatory sequences in all *bin3*-expressing
153 tissues, not just in the ovary. To do this, we used BAC clone CH322-154G8 (BACPAC Genomics) that
154 comprises a 22.065 kb fragment of chromosome 2R, containing the *bin3* P1 promoter (Singh *et al.*
155 2011), and 3 of the 4 predicted mRNA isoforms of *bin3* (*bin3-RA*, *bin3-RC*, and *bin3-RD*). This BAC was
156 inserted into the *attP* landing site on chromosome 3R in BDSC stock #9744 (y^1 w^{1118}; *PBac{*y^+*-attP-*
157 *9A}VK00027*) by BestGene, Inc.
158

159 **Generation of the pUAS-DSCP-XbaI-attB vector via NEBuilder HiFi DNA Assembly**

160 High-copy plasmids pNP (Qiao *et al.* 2018; Wang *et al.* 2019) and pUASP-attB (Drosophila Genomics
161 Resource Center Stock 1358; https://dgrc.bio.indiana.edu//stock/1358; RRID:DGRC_1358; Takeo *et al.*
162 2012) were purified from bacterial cells grown to confluence at 37°C in LB + 100 µg/ml ampicillin using
163 the Monarch Plasmid Miniprep Kit T1010L from New England BioLabs, Inc. (NEB). To create pUAS-
164 DSCP-XbaI-attB (the vector into which *bin3* and 3xHA sequences would be cloned, see below), the
165 10XUAS-DSCP promoter was amplified from plasmid pNP with Q5 High-Fidelity DNA Polymerase
166 (NEB) using primers UP0394 and UP0395, and inserted into pUASP-attB that had been digested with
167 *Xho*I (NEB) and *Pst*I (NEB), via NEBuilder HiFi DNA Assembly (NEB.). NEBuilder HiFi DNA Assembly
168 destroyed the *Xho*I site, and partially eliminated one of the two GAGA enhancers in pUASp-attB .
169

170 **Ovarian RNA Purification and Reverse Transcription for NEBuilder HiFi DNA Assembly**

171 one to three-day old w^{1118} (BDSC #5905) females were incubated with males in yeasted vials overnight.
172 Five pairs of ovaries were dissected from two to four-day old females in ice-cold 1X PBS, and flash-
173 frozen in liquid nitrogen. Total RNA was extracted using the Monarch Total RNA Miniprep Kit (NEB),
174 according to the manufacturer's instructions for RNA purification from "Tissues". Total RNA (1 µg) was

175 reverse transcribed using ProtoScript II First Strand cDNA Synthesis Kit (NEB, E6560S) with primer
176 UP0118, which anneals to the very end of *bin3* coding sequence (CDS). See **Table S4** for primer
177 sequence.
178
179 **Purification of BAC clone CH322-154G8 for NEBuilder HiFi DNA Assembly**
180 EPI300 bacterial cells (Lucigen) harboring the BAC clone CH322-154G8 (BACPAC Genomics) were
181 grown to confluence at 37°C in LB + 12.5 µg/ml chloramphenicol, and plasmid replication was induced
182 by diluting 1:10 in LB + 12.5 µl/ml chloramphenicol and 1X CopyControl Induction Solution (Lucigen).
183 The BAC was purified purified using the Monarch Plasmid Miniprep Kit (NEB).
184
185 **Generation of *UAS-DSCP-3xHA-bin3* transgenic flies via NEBuilder HiFi DNA Assembly**
186 To generate plasmid *pUAS-DSCP-3xHA-bin3-attB*, which expresses Bin3 C-terminally tagged with 3xHA,
187 under UAS control: Fragment #1, comprising the *bin3-RA* 5′-UTR to the end of the *bin3* CDS, was
188 amplified from *bin3* cDNA using Q5 High-Fidelity DNA Polymerase, and primers UP0423 and UP0414.
189 The 5′ end of Fragment #1 is homologous to sequences immediately upstream of the *Xba*I site in pUAS-
190 DSCP-XbaI-attB; the 3′ end of Fragment #1 is homologous to 5′ end of a synthetic dsDNA fragment
191 comprising Gly-Gly-Gly-Ser-3xHA (G_4S-3xHA; Integrated DNA Technologies) codon-optimized for
192 *Drosophila* with the IDT Codon Optimization Tool (Integrated DNA Technologies). Fragment #2,
193 comprising the entire *bin3-RA* 3′-UTR, was amplified from the BAC clone CH322-154G8 using Q5 High-
194 Fidelity DNA Polymerase, and primers UP0415 and UP0424. The 5′ end of Fragment #2 is homologous
195 to the 3′ end of the G_4S-3xHA fragment; the 3′ end of Fragment #2 is homologous to sequences
196 immediately downstream of the *Xba*I site in pUAS-DSCP-XbaI-attB. Fragment #1, G_4S-3xHA, and
197 Fragment #2 were assembled in this order into the *Xba*I site of pUAS-DSCP-XbaI-attB via NEBuilder
198 HiFi DNA Assembly. The *Xba*I site was destroyed.

To generate plasmid *pUAS-DSCP-3xHA-bin3*^{Y795A}*-attB*, which expresses catalytically-dead Bin3^{Y795A}, C-terminally tagged with 3xHA ,under UAS control: Fragment #3, comprising the *bin3-RA* 5′-UTR to 11 nt downstream of the Y795 codon, was amplified from *bin3* cDNA using Q5 High-Fidelity DNA Polymerase, and primer UP0423 and the mutagenic primer UP0419, which introduces a Y795A point mutation. The 5′ end of Fragment #3 is homologous to sequences immediately upstream of the *Xba*I site in pUAS-DSCP-XbaI-attB; the 3′ end of Fragment #3 is homologous to the 5′ end of Fragment #4. Fragment #4, comprising 11 nt upstream of the Y795 codon to the end of the *bin3-RA* CDS was amplified from cDNA using Q5 High-Fidelity DNA Polymerase, and mutagenic primer UP0420, which introduces a Y795A point mutation, and primer UP0414. The 5′ end of Fragment #4 is homologous to the 3′ end of Fragment #3; the 3′ end of Fragment #4 is homologous to 5′ end of the G_4S-3xHA fragment. Fragment #3, Fragment #4, G_4S-3xHA, and Fragment #2 (see above) were assembled in this order into the *Xba*I site of pUAS-DSCP-XbaI-attB via NEBuilder HiFi DNA Assembly. The *Xba*I site was destroyed.

To generate plasmid *pUAS-DSCP-3xHA-bin3*$^{\Delta MSM}$*-attB*, which expresses Bin3$^{\Delta MSM}$, C-terminally tagged with 3xHA, under UAS control: Fragment #5, comprising the *bin3-RA* 5′-UTR to 12 nt downstream of the L326 codon, was amplified from *bin3* cDNA using Q5 High-Fidelity DNA Polymerase, and primer UP0423 and the mutagenic primer UP0417, which eliminates codons 311-326. The 5′ end of Fragment #5 is homologous to sequences immediately upstream of the *Xba*I site in pUAS-DSCP-XbaI-attB; the 3′ end of Fragment #5 is homologous to the 5′ end of Fragment #6. Fragment #6, comprising 12 nt upstream of the F311 codon to the end of the *bin3-RA* CDS was amplified from cDNA using Q5 High-Fidelity DNA Polymerase and mutagenic primer UP0418, which eliminates codons 311-326, and primer UP0414. The 5′ end of Fragment #6 is homologous to the 3′ end of Fragment #5; the 3′ end of

Fragment #6 is homologous to 5′ end of the G_4S-3xHA fragment. Fragment #5, Fragment #6, G_4S-3xHA, and Fragment #2 (see above) were assembled in this order into the *Xba*I site of pUAS-DSCP-XbaI-attB via NEBuilder HiFi DNA Assembly. The *Xba*I site was destroyed.

See **Table S4** for primer sequences and the sequence of the G_4S-3xHA synthetic dsDNA fragment used to make these 3 constructs. Sequencing of each construct revealed that all UTRs corresponded to the *bin3-RA* mRNA isoform of *bin3*. Interestingly, each construct had an in-frame insertion of an Ala residue between L573 and V574, when mapped to the reference sequence of *bin3* (NCBI Reference Sequence NM_165468.2). These 3 constructs were recombined into the *attP* landing site on chromosome 3L in BDSC stock #8622 (y^1 w^{67c23}; $P\{y^{+t7.7}$=*CaryP*}*attP2*) by BestGene, Inc.

Expression of *UAS-DSCP-3xHA-bin3* transgenes using the Trojan GAL4 approach

We used the UAS/GAL4 system (Brand and Perrimon 1993) and the Trojan GAL4 approach (Diao and White 2012; Diao *et al.* 2015; Lee *et al.* 2018) to induce the expression of *UAS-DSCP-3xHA-bin3* (hereon referred to as *UAS-bin3*) transgenes. Intronic Trojan GAL4 insertions produce a null allele of a gene while also expressing GAL4 under the regulatory sequences of that gene. A Trojan GAL4 insertion into one of the *bin3* introns ($bin3^{MI08045\text{-}TG4.0}$, hereon referred to as $bin3^{TG4.0}$) in *trans* to a deficiency (*Df*) uncovering *bin3* produces *bin3*-null ($bin3^{TG4.0}/Df$) flies that express GAL4 in the spatiotemporal pattern of endogenous *bin3*. (**Fig. 4a**). When transgenes comprising *UAS-bin3* cDNAs (**Fig. 5d-f**) are incorporated into $bin3^{TG4.0}/Df$ flies, GAL4 induces expression of Bin3 proteins in the pattern of endogenous *bin3* in an otherwise *bin3*-null background.

Total RNA purification from ovaries and RT-qPCR

Five one to three-day old females were incubated with males in yeasted vials overnight. Five pairs of ovaries were dissected from two to four-day old females in ice-cold 1X PBS, and flash-frozen in liquid nitrogen. Total RNA was extracted using the Monarch Total RNA Miniprep Kit (NEB), according to the manufacturer's instructions for RNA purification from "Tissues". RT-qPCR was performed on 10 ng total RNA using the Luna Universal One-Step RT-qPCR Kit (NEB, E3005L). *bin3*, 7SK, U6, and *rp49* mRNAs were reverse transcribed and amplified with primers UP0493 + UP0118, UP0146 + UP0147, OW1123 + OW1124, and UP0113 + UP0114, respectively (see **Table S4** for primer sequences). Reactions were performed using a CFX Opus 384 Real-Time PCR System (Bio-Rad).

Protein extraction and Western Analysis

Ten one to three-day old females were incubated with males in yeasted vials overnight. Ten pairs of ovaries were dissected from two to four-day old females in ice-cold 1X PBS, and flash-frozen in liquid nitrogen. Protein was exacted as previously described {Prudêncio.2015}. Extracts were clarified through 0.22 µM Spin-X columns (Costar), and mixed 1:1 with 2X Sample Loading Buffer (Bio-Rad) + 5% β-mercaptoethanol, and boiled for 5 minutes. Extracts were spun down, and 15 µl was loaded onto 4-20% TGX gels (Bio-Rad), and ran at 100 V for 10 minutes, then 300 V for 20 minutes. Protein was transferred to PVDF-LF membranes (Bio-Rad) using a Trans-Blot Turbo Transfer System (Bio-Rad) using the High MW preset (1.3 A, 25 V, 10 minutes). Membranes were blocked in EveryBlot Blocking Buffer (Bio-Rad) for 5 minutes, and then incubated with primary antibodies diluted in EveryBlot Blocking Buffer for 1 hour at room temperature. Membranes were washed with TBST (1X Tris-Buffered Saline, 0.2% Tween-20) for 5 minutes 3 times, and then incubated with secondary antibodies diluted in EveryBlot Blocking Buffer for 1 hour at room temperature. Membranes were with TBST for 5 minutes 3 times, dehydrated with 100% methanol, and imaged using a ChemiDoc MP Imaging System with Image Lab Touch software (Bio-Rad). Primary antibodies used were 1 µg/ml rabbit anti-HA (abcam, ab9110), and 1 µg/ml

mouse anti-beta Actin (abcam, ab170325), and 5 µg/ml IgG purified from sheep anti-CycT antiserum (Nguyen *et al.* 2012). using Pierce Protein G Magnetic Beads according to the manufacturer's instructions. Secondary antibodies were from Jackson ImmunoResearch, Inc., and used at 1 µg/ml: Alexa Fluor 488 AffiniPure Donkey Anti-Rabbit IgG (711-545-152), Alexa Fluor 488 AffiniPure Donkey Anti-Sheep IgG (713-545-147), Alexa Fluor 594 AffiniPure Donkey Anti-Mouse IgG (715-585-150), and Alexa Fluor 647 AffiniPure Donkey Anti-Mouse IgG (715-605-150).

Egg-Laying Assay

Ten one to three-day old virgin females were incubated with wild-type males *en masse* in yeasted vials overnight. Ten two to four-day old females were split individually into fresh vials with two Oregon-R males, and incubated for 24 hours. After 24 hours, eggs were counted to determine the number of eggs laid/female/day. Experiments were performed in biological triplicate.

Immunofluorescence staining of ovaries

Immunofluorescence staining of ovaries was performed as described (Maimon and Gilboa 2011). Ten 1-4 day old females were incubated with males in yeasted vials overnight, and then 10 pairs of ovaries were dissected from 2-5 day old females in ice-cold 1X PBS. The following steps were performed at RT unless otherwise indicated. Ovaries were fixed in 1 ml of Image-iT Fixative Solution (Thermo Scientific, R37814) + 0.3% Triton X-100 for 20 minutes. Ovaries were washed and permeabilized with 1 ml of 1% PT Buffer (1X PBS, 1% Triton X-100) for 5 minutes, 10 minutes, and 45 minutes. Ovaries were blocked with 1 ml PBT (1X PBS, 1% BSA, 0.3% Triton X-100) for 1 hour, and then incubated in 250 µl PBT and primary antibodies overnight at 4°C. Primary antibodies used were 1 µg/ml rabbit anti-HA (abcam ab9110) and 5 µg/ml mouse anti-Vasa (Developmental Studies Hybridoma Bank, Vasa 46F11). Ovaries were washed with 1 ml 0.3% PT Buffer (1X PBS, 0.3% Triton X-100) 3 times for 30 minutes each, blocked with 1 ml

294 PBT-NDS (1X PBS, 1% BSA, 0.3% Triton X-100, 5% normal donkey serum) for 1 hour, and incubated in
295 250 µl PBT-NDS containing 10 µg/ml Hoechst 33342 (Thermo Scientific, H3570) and 2 µg/ml secondary
296 antibodies for 2 hour in the dark. Secondary antibodies were from Jackson ImmunoResearch, Inc.:
297 Alexa Fluor 488 AffiniPure Donkey Anti-Rabbit IgG (711-545-152) and Alexa Fluor 647 AffiniPure Donkey
298 Anti-Mouse IgM (715-605-020). Ovaries were washed with 1 ml 0.3% PT Buffer in the dark 3 times for 30
299 minutes each, then mounted in 50 µl VECTASHIELD PLUS Antifade Mounting Medium (Vector Labs,
300 Inc., H-1900-10).
301
302 **Single-molecule fluorescence *in situ* hybridization (smFISH) in ovaries**
303 smFISH on adult ovaries was performed essentially as described (Raj and Tyagi 2010; Abbaszadeh and
304 Gavis 2016). Ten 1-4 day old females were incubated with males in yeasted vials overnight, and then 10
305 pairs of ovaries were dissected from 2-5 day old females in ice-cold 1X PBS. The following steps were
306 performed at RT unless otherwise indicated. Ovaries were fixed in 1 ml of Image-iT Fixative Solution
307 (Thermo Scientific, R37814) for 30 minutes, then washed with PBST (1X PBS, 0.1% Tween-20) 3 times
308 for 5 minutes each. Ovaries were permeabilized by incubating in 7:3 PBST:methanol for 5 minutes, 1:1
309 PBST:methanol for 5 minutes, 3:7 PBST:methanol for 5 minutes, 100% methanol for 10 minutes, 3:7
310 PBST:methanol for 5 minutes, 1:1 PBST:methanol for 5 minutes, and 7:3 PBST:methanol for 5 minutes.
311 Ovaries were then washed with PBST 4 times for 5 minutes each, followed by pre-hybridized in Wash
312 Buffer A (20% Stellaris RNA FISH Wash Buffer A (Biosearch Technologies Cat# SMF-WA1-60) and 10%
313 deionized formamide) for 5 minutes. Ovaries were incubated in Stellaris RNA FISH Hybridization Buffer
314 (Biosearch Technologies Cat# SMF-HB1-10) with 10% deionized formamide and 125 µM Quasar 640-
315 labeled oligonucleotide probes, overnight at 37°C in the dark. Oligonucleotide probes against 7SK were
316 designed using the LGC Biosearch Technologies' Stellaris RNA FISH Probe Designer
317 (https://www.biosearchtech.com/support/tools/design-software/stellaris-probe-designer). Ovaries

were washed in the dark with Wash Buffer A for 30 minutes at 37°C, and then with Wash Buffer A with 10 µg/ml Hoechst 33342 (Thermo Scientific, H3570) for 30 minutes at 37°C, and finally with Stellaris RNA FISH Wash Buffer B (Biosearch Technologies Cat# SMF-WB1-20) for 5 minutes at RT. Ovaries were mounted in 50 µl VECTASHIELD PLUS Antifade Mounting Medium (Vector Labs, Inc., H-1900-10).

Ovariole Counting Assay

One to three-day old females were incubated with sibling males in yeast vials overnight. Two to four-day females were anesthetized, transferred to 1.7 ml tubes, flash-frozen in liquid nitrogen, and stored at -80°C. Frozen females were thawed on ice or at RT and dissected in a 1:1 mixture of methanol and 1X PBS. 50% methanol dehydrates and extracts lipids from the gonadal sheath surrounding the ovary and from the clear portions of the ovarioles (turning them opaque), making ovarioles easy to separate and count. The mean number of ovarioles per ovary, as well as the absolute value of the difference in ovariole number between each ovary per female were calculated (Lobell *et al.* 2017). Experiments were performed in biological duplicate.

Climbing Assay

Ten 2-5 day old females were transferred to 15 ml tubes, and allowed to acclimate for 3′. Flies were tapped to the bottom of the tube, and climbing was recorded for 12 seconds. Flies were then allowed to reacclimatize for another 3 minutes before performing the subsequent trial. 10 trials were performed per genotype to determine the percent of flies climbing 8 cm in 12 seconds per trial. All genotypes for a particular experiment were tested at the same time. Experiments were performed in biological triplicate.

Modeling of Bin3 protein sequence onto MEPCE

342 Bin3 was modeled onto 309 amino acids of the MEPCE active site in complex with *S*-adenosyl-
343 homocysteine (SAH) and stem loop 1 of 7SK (PDB 6dcb; Yang *et al.* 2019) using hhpred (Söding 2005;
344 Hildebrand *et al.* 2009; Meier and Söding 2015; Zimmermann *et al.* 2018; Gabler *et al.* 2020) and
345 MODELLER (Šali *et al.* 1995; Zimmermann *et al.* 2018; Gabler *et al.* 2020). Alignment of the Bin3 model
346 to 6dcb, RMSD calculation, and modeling of the Y421A and Y795A mutations was performed using
347 PyMol (version 2.5.4).
348
349 **Bin3 Disorder Prediction**
350 Disorder in Bin3 was predicted by IUPred3, using the IUPred3 short disorder analysis type (Mészáros *et*
351 *al.* 2018; Erdős and Dosztányi 2020; Erdős *et al.* 2021).
352
353 **RNA Immunoprecipitation (RIP)**
354 Twenty-five one to three-day old females with or without transgenes expressing *bin3-3xHA* cDNAs
355 were incubated with males in yeasted vials overnight. Twenty-five pairs of ovaries were dissected from
356 two to four-day old females in ice-cold, 1X PBS, and fixed in 1 ml 1.8% formaldehyde (a mixture of 55%
357 1X PBS and 45% Image-iT Fixative Solution, Thermo Scientific, R37814) for 15 minutes at RT on a
358 nutating rotor. Fixation was terminated by addition of 163 µl 2.5 M glycine to a final concentration of
359 ~350 mM, and incubation for 5 minutes at RT on a nutating rotor. Ovaries were washed briefly with with
360 1X PBS 3 TIMES, and then flash-frozen in liquid nitrogen. Ovaries were homogenized by hand with a
361 blue pestle on ice in 50 µl ice-cold RIPA Lysis and Extraction Buffer (Thermo Scientific, 89900)
362 supplemented with 1 mM DTT, 3X Halt Protease and Phosphatase Inhibitor Cocktail (Thermo Scientific,
363 78440), and 1 U/µl SUPERase•In RNase Inhibitor (Invitrogen, AM2696). 200 µl of additional buffer was
364 added to the homogenate, and samples were incubated on ice for 15 minutes to allow for complete
365 nuclear lysis. Homogenate was pelleted by centrifugation at top speed for 1 minute. 2.5 µl of

homogenate (1/100th homogenate volume) was removed and kept on ice in a total of 300 µl 1X Monarch DNA/RNA Protection Reagent (NEB, T2011L) as the input sample. The remaining homogenate was used for immunoprecipitation. 25 µl (1/10th homogenate volume) of Pierce Anti-HA Magnetic Beads (Thermo Scientific, 88836) were washed with 175 µl 1X TBS-T (Pierce 20X TBS Tween 20 Buffer, Thermo Scientific, 28360), and then with 1 ml 1X TBS-T. Homogenate was added to the washed beads, and immunoprecipitation was performed for 4 hours at 4°C with end-over-end rotation. Beads were washed briefly with 1 ml 1X TBS-T 3 times. Bin3-3xHA complexes were purified by two sequential competitive elutions with 75 µl of Pierce HA Peptide (Thermo Scientific, 26184) diluted to 2 mg/ml in Nuclease-Free Water (NEB, B1500L), at 37°C for 15 minutes each. The eluates were pooled, and the 150 µl total eluate was added to 150 µl 2X Monarch DNA/RNA Protection Reagent. All samples (inputs and eluates) were incubated at 65-70°C for 30 minutes to reverse formaldehyde crosslinks. Total RNA was extracted using the Monarch Total RNA Miniprep Kit (NEB), according to the manufacturer's instructions for RNA purification from "Tissues". Total RNA was eluted in 100 µl Nuclease-Free Water. 2.9 µl of each sample was used in 10-µl reactions to reverse transcribe and amplify 7SK and U6 snRNAs with primers UP0146 + UP0147 and OW1123 + OW1124, respectively (see **Table S4** for primer sequences). Reactions were performed using the Luna Universal One-Step RT-qPCR Kit (NEB, E3005L) and a CFX Opus 384 Real-Time PCR System (Bio-Rad).

RESULTS

Bin3 is required for female fecundity

Reproductive success is influenced by fertility (offspring viability) and fecundity (the rate of offspring production). Previously, we showed that Bin3 plays a role in fertility, promoting embryonic viability by a mechanism of *caudal* translation repression (Singh *et al.* 2011). During that and other studies, we noticed that *bin3* mutants lay fewer eggs than wild type flies. Therefore, we asked if Bin3 also plays a role in fecundity by promoting a normal egg-laying rate. To do this, we compared the egg-laying rates of flies that were either wild type for *bin3* (wt), heterozygous for *bin3* ($bin3^{2-7}$/+), or deleted entirely for *bin3* ($bin3^{2-7}$ in *trans* to a deficiency that removes the *bin3* locus; $bin3^{2-7}/Df$). The genomic regions deleted by $bin3^{2-7}$ and *Df* are depicted in **Fig. 1a**. As expected, *bin3* mRNA levels are reduced by half in $bin3^{2-7}$/+ heterozygotes and are undetectable in $bin3^{2-7}/Df$ mutants (**Fig. 1b**). Interestingly, we found that $bin3^{2-7}/Df$ females laid eggs at a significantly reduced rate compared to wt ($P = .0001$) and $bin3^{2-7}$/+ ($P < .0001$) females (**Fig. 2a**). The egg-laying rate defect was specific to the loss of *bin3*, as a single copy of a genomic fragment containing the *bin3* ORF ($bin3^{+}$, **Fig. 1a**) restored *bin3* mRNA accumulation by half (**Fig. 1b**) and rescued the egg-laying defect of $bin3^{2-7}/Df$ females ($P < .0001$, **Fig. 2a**). Rescue was comparable to that of $bin3^{2-7}$/+ controls. These results demonstrate that Bin3 is required for egg-laying.

Bin3 promotes female fecundity by repressing P-TEFb

We found that 7SK RNA levels were strongly reduced in $bin3^{2-7}/Df$ females compared to wt ($P < .0001$, **Fig. 1c**), as we have previously shown (Singh *et al.* 2011). The canonical function of Bin3/MEPCE is to stabilize 7SK RNA (Jeronimo *et al.* 2007; Singh *et al.* 2011). 7SK RNA in turn acts as a scaffold for proteins that form a snRNP that sequesters and represses P-TEFb (Krueger *et al.* 2008; Barboric *et al.* 2009; Xue *et al.* 2010; Muniz *et al.* 2013; Brogie and Price 2017; Yang *et al.* 2022). Therefore,

407 destabilization of 7SK in *bin3*$^{2\text{-}7}$/*Df* females should lead to deregulation (activation) of P-TEFb, which
408 could be responsible for the egg-laying defect. If this is true, then we expect that reducing the activity
409 of P-TEFb in *bin3*$^{2\text{-}7}$/*Df* females would rescue the egg-laying defect. To genetically reduce the activity of
410 P-TEFb, we introduced a mutant allele of *CycT* (*CycT*^{jIIB2}) into *bin3*$^{2\text{-}7}$/*Df* flies, and confirmed that this
411 mutation reduces the protein levels of the largest of the two CycT isoforms (**Fig. 1e**). Indeed, we found
412 that reducing the amount of CycT in *bin3*$^{2\text{-}7}$/*Df* females rescued the egg-laying defect (P < .0001, **Fig.**
413 **2a**), while having no effect on 7SK RNA levels (**Fig. 1c**). These results suggest that Bin3 stabilizes 7SK
414 RNA to form the 7SK snRNP, which then sequesters and represses P-TEFb to promote a normal egg-
415 laying rate.
416
417 **Bin3 and 7SK are expressed ubiquitously in the ovary**
418 To gain insight into the role of Bin3 in egg-laying, we determined where Bin3 (and its substrate
419 7SK) is expressed and localized in ovaries, which are composed of 16-20 individual ovarioles that can be
420 thought of as assembly lines of germline development (**Fig. 2b**). We used the UAS/GAL4 (Brand and
421 Perrimon 1993) and Trojan GAL4 systems (see Materials and Methods; Diao and White 2012; Diao *et al.*
422 2015; Lee *et al.* 2018), where a Trojan GAL4 insertion into the *bin3* ORF was used to drive the expression
423 of a 3xHA-epitope-tagged *bin3* transgene in the spatiotemporal pattern of endogenous *bin3* (*bin3*$^{TG4.0}$ >
424 *UAS-3xHA-bin3*). Bin3-3xHA was detected by immunofluorescence staining of ovaries. We found that
425 Bin3 is expressed in and localized to the nucleic of all ovarian cells (**Fig. 2, c, c'**). Bin3 was found to be
426 expressed in the germline cells of the germarium (located at the anterior of each ovariole), and in the 15
427 nurse cells that supply the oocyte with mRNAs and proteins. Bin3 was also found to be expressed in the
428 somatic cells surrounding the germline cells and the oocyte, which communicate with germline cells to
429 promote egg chamber and oocyte maturation. Control flies lacking the *UAS-3xHA-bin3* transgene
430 (*bin3*$^{TG4.0}$/+) yielded no detectable HA staining (**Fig. 2, d, d'**).

To identify where in the ovary 7SK RNA is expressed and localized, we performed single-molecule fluorescence *in situ* hybridization (Raj and Tyagi 2010; Abbaszadeh and Gavis 2016) on ovaries from wt and *bin3*$^{2-7}$*/Df* females. We found that in wt ovarioles, 7SK follows an identical expression pattern to that of Bin3 (compare **Fig. 2, e, e'** with **Fig. 2, c, c'**). As expected, 7SK staining was undetectable in *bin3*$^{2-7}$*/Df* ovarioles (**Fig. 2, f, f'**), which do not accumulate 7SK RNA (**Fig. 1c**). Taken together, Bin3 and 7SK are both expressed in all cells of the ovarioles and localize to nuclei—commensurate with their role in transcription elongation regulation.

Bin3 is not required to establish the proper number of ovarioles

The total number of ovarioles per ovary directly correlates with the number of eggs insects can lay (Wayne *et al.* 1997; Wayne and Mackay 1998), and is established by proper proliferation and migration of the somatic terminal filament cells (TFCs; Sahut-Barnola *et al.* 1995, 1996). Given that we found *bin3*$^{2-7}$*/Df* mutant females had an egg-laying defect, and that Bin3 is expressed in the somatic cells of the ovarioles, we hypothesized that Bin3 promotes egg-laying by functioning in the TFCs to establish ovarioles. To test this hypothesis, we used the UAS/GAL4 system (Brand and Perrimon 1993) with two different *bab1-GAL4* drivers (Cabrera *et al.* 2002) to induce expression of the *UAS-3xHA-bin3* transgene specifically in the somatic TFCs of *bin3*$^{2-7}$*/Df* females to determine whether this rescued the egg-laying rate. Unfortunately, we were unable to recover *bin3*$^{2-7}$*/Df; bab1-GAL4/UAS-bin3* flies using either driver. Both *bab1-GAL4* drivers are expressed in several cell types in addition to the TFCs (Cabrera *et al.* 2002), and therefore it is likely that ectopic expression of *bin3* in all *bab1*-expressing cells is lethal.

As an alternative approach, we compared ovariole numbers in *bin3*$^{2-7}$*/Df* females with those of wt and *bin3*$^{2-7}$/+ controls. To do this, we dissected ovaries and determined (i) the average number of ovarioles per ovary, and (ii) the difference in the number of ovarioles within a pair of ovaries (i.e., "ovariole asymmetry"; Lobell *et al.* 2017). Unexpectedly, we did not find a significant difference in

either the mean number of ovarioles per ovary (**Fig. 2g**) or in ovariole asymmetry (**Fig. 2h**) in *bin3*$^{2-7}$*/Df* females compared to either wt or *bin3*$^{2-7}$/+ control females.

Together, these results suggest that Bin3 is not required to establish ovarioles, and therefore promotes egg-laying by some other mechanism. These results also suggest that Bin3 does not have a function in TFCs relevant to the establishment of ovarioles. However, these results do not rule out some other function of Bin3 in TFCs (*e.g.*, cell-cell communication with germline cells) that might promote egg-laying. The lethality of inducing *bin3* expression in TFCs using the *bab1-GAL4* drivers precludes the ability to test this hypothesis in any straightforward way.

Expression of Bin3 in the germline is not sufficient to promote fecundity

Bin3 is also expressed in germline cells, therefore, it remained possible that Bin3 functions in the germline to promote a normal egg-laying rate. To test this hypothesis, we used a *nanos-GAL4::VP16* driver (Doren *et al.* 1998) to induce expression of the *UAS-3xHA-bin3* transgene specifically in the germline cells of *bin3*$^{2-7}$*/Df* females, and asked whether this improved the egg-laying rate (**Fig. 2g**). Results showed that germline expression of *bin3* did not rescue the egg-laying rate defect of *bin3*$^{2-7}$*/Df; nanos-GAL4::VP16/UAS-bin3* females compared to *bin3*$^{2-7}$*/Df; nanos-GAL4::VP16/*+ mutant females (P = .9942, **Fig. 2i**), suggesting that Bin3 does not function in germline cells to promote a normal egg-laying rate.

Bin3 has a conserved role in neuromuscular function

A nonsense mutation in the *MEPCE* gene of a patient with impaired neuromuscular ability was shown to reduce MEPCE protein levels, causing P-TEFb hyper-activation and aberrant RNAPII transcription elongation (Schneeberger *et al.* 2019). If a conserved function of Bin3/MEPCE is to repress P-TEFb to promote normal neurodevelopment, then it would be expected that *bin3* mutant flies would

479 also have neuromuscular defects, and that these defects should be rescued by reducing CycT levels
480 (lowering P-TEFb activity).
481 Two ways in which neuromuscular function can be assessed in flies is by examining climbing
482 (Manjila and Hasan 2018) and resting wing posture (Baehrecke 1997). Normally, flies climb to the top of
483 an enclosure after being knocked to the bottom, and fold their wings one-over-the-other when resting.
484 We found that a significant percentage of *bin3*$^{2-7}$*/Df* flies had a climbing defect compared to *bin3*$^{2-7}$/+
485 control flies (P = .0003, **Fig. 3a**). Additionally, whereas control *bin3*$^{2-7}$/+ flies properly folded their wings
486 (**Fig. 3b**), *bin3*$^{2-7}$*/Df* mutant flies had a *held-out wings* phenotype (**Fig. 3c**). Both defects were specific to
487 loss of *bin3*, as the *bin3*$^{+}$ genomic fragment rescued the climbing (*P* = .0004, **Fig. 3a**) and resting wing
488 posture defects of *bin3*$^{2-7}$*/Df* flies (compare **Fig. 3d** with **Fig. 3c**). Importantly, both climbing (*P* = .0008,
489 **Fig. 3a**) and wing posture (compare **Fig. 3e** with **Fig. 3c**) defects of *bin3*$^{2-7}$*/Df* flies were also rescued by
490 reducing CycT levels. These results suggest that Bin3 and MEPCE share a conserved role in
491 neuromuscular function from *Drosophila* to humans, most likely by repressing P-TEFb and preventing
492 aberrant transcription elongation.
493
494 **Bin3 catalytic activity is dispensable for 7SK stability and snRNP function *in vivo***
495 The importance of MEPCE catalytic residues in 7SK binding and capping have been studied
496 mostly *in vitro* (Xue *et al.* 2010; Shelton *et al.* 2018; Yang *et al.* 2019). To determine the importance of
497 Bin3 catalytic activity *in vivo,* we sought to generate flies expressing a catalytically-dead Bin3 protein.
498 We first analyzed the crystal structure of the methyltransferase domain of human MEPCE (PDB 6dcb,
499 Yang *et al.* 2019). As shown in **Fig. 4a,** Tyrosine 421 (Y421) is juxtaposed between the 5′ gamma
500 phosphate of 7SK and S-adenosyl-homocysteine (SAH; used in place of the S-adenosyl-methionine
501 (SAM) methyl donor for the purposes of crystallization). Y421 hydrogen bonds to the 7SK gamma
502 phosphate. Mutation of this tyrosine to alanine (Y421A) completely abolished MEPCE catalytic activity

503 *in vitro* (Yang *et al.* 2019). We modeled Bin3 onto the crystal structure (**Fig. 4a**) and found that Y795 in
504 Bin3 (red) aligned well with Y421 in MEPCE (black). We created models (**Fig. 4b**) representing the
505 Y421A mutation in MEPCE (black) and the concomitant Y795A mutation in Bin3 (red), which revealed a
506 complete loss of coordination between 7SK, SAH (i.e., SAM), and MEPCE/Bin3.

507 Given the *in vitro* importance of the Y421 residue in MEPCE for catalytic activity, and that Y795
508 in Bin3 aligns with Y421, we generated flies expressing either wt Bin3 ($Bin3^{wt}$) or $Bin3^{Y795A}$ and tested
509 whether $Bin3^{Y795A}$ was able to (i) bind and stabilize 7SK, and (ii) rescue *bin3* mutant phenotypes. To do
510 this, we again used the Trojan GAL4 approach. Importantly, not only do Trojan GAL4 insertions express
511 GAL4 in the pattern of the gene they are inserted into, but they simultaneously generate a null allele of
512 the inserted gene. Indeed, *bin3* Trojan GAL4 insertion flies ($bin3^{TG4.0}/Df$) (**Fig. 4d**) had nearly
513 undetectable levels of both *bin3* mRNA ($P < .0001$, **Fig. 4e**) and 7SK RNA ($P < .0001$ **Fig. 4f**) compared to
514 wt, confirming that $bin3^{TG4.0}$ is a null allele of *bin3*. Additionally, we found that GAL4 expressed from
515 $bin3^{TG4.0}$ induced both $UAS\text{-}bin3^{wt}$ (**Fig. h**) and $UAS\text{-}bin3^{Y795A}$ (**Fig. 4i**) transgenes similarly at the mRNA
516 ($P = .2188$, **Fig. 4k**) and protein ($P = .9836$, **Fig. 4l**) levels. Thus, these flies could be used to study the
517 importance of Bin3 catalytic activity *in vivo*.

518 Bin3 catalytic activity is expected to be required for capping and stabilization of 7SK *in vivo*;
519 therefore, in $Bin3^{Y795A}$ mutant flies, 7SK should be destabilized. Remarkably, there was no significant
520 difference in 7SK levels between $Bin3^{Y795A}$ flies ($bin3^{TG4.0}/Df$; $UAS\text{-}bin3^{Y795A}/+$) and $Bin3^{wt}$ flies ($bin3^{TG4.0}/Df$;
521 $UAS\text{-}bin3^{wt}/+$; $P = .9996$, **Fig. 5a**), suggesting that Bin3 catalytic activity is not required for the stability
522 of 7SK *in vivo*. How then might Bin3 stabilize 7SK in the absence of catalytic activity? As suggested by
523 prior studies (Xue *et al.* 2010), Bin3 might form a stable complex with 7SK independent of its catalytic
524 function, and this may protect it from degradation. Indeed, we find that $Bin3^{Y795A}$ immunoprecipitated
525 as much 7SK RNA as did $Bin3^{wt}$ ($P = .5350$, **Fig. 5b**), suggesting that the Y795A mutation does not
526 diminish the binding of Bin3 to 7SK, and that binding alone is sufficient for stabilization *in vivo*.

527 Given that Bin3^{Y795A} could bind and stabilize 7SK, we expected that Bin3^{Y795A} would rescue the
528 fecundity, climbing, and wing posture defects of *bin3* mutant flies. First, we showed that *bin3*$^{TG4.0}$*/Df*
529 flies recapitulate the fecundity (compare **Fig. 6a** to **Fig. 2a**), climbing (compare **Fig. 6b** with **Fig. 3a**),
530 and wing posture (compare **Fig. 6d** with **Fig. 3c**) defects of *bin3*$^{2-7}$*/Df* flies. As expected, Bin3^{Y795A}
531 expression rescued the fecundity (P = .0008, **Fig. 6a**), climbing (P < .0001, **Fig. 6b**), and wing posture
532 (compare **Fig. 6f** to **Fig. 6d**) defects of *bin3*$^{TG4.0}$*/Df* flies, similar to Bin3^{wt} (P > .9999 for both fecundity
533 and climbing). Therefore, despite the importance of catalytic activity to 7SK capping *in vitro*, Bin3
534 catalytic activity and therefore the methylphosphate cap do not seem to be required *in vivo* for 7SK
535 stability, nor is it likely to affect 7SK snRNP assembly and function (**Fig. 6i**).
536
537 **A metazoan-specific motif in Bin3 is required to promote specific neuromuscular functions**
538 Much attention has been given to the methyltransferase domain of Bin3 orthologs; however,
539 metazoans have acquired over evolutionary time additional protein sequences outside of the
540 methyltransferase domain (Cosgrove *et al.* 2012). To determine whether there is conserved homology
541 between Bin3 orthologs in these regions, we aligned several Bin3 orthologs that have been previously
542 characterized, including *Drosophila* Bin3 (Zhu and Hanes 2000; Singh *et al.* 2011; Cosgrove *et al.* 2012),
543 human MEPCE (Xue *et al.* 2010; Muniz *et al.* 2013; Shelton *et al.* 2018; Schneeberger *et al.* 2019; Yang *et*
544 *al.* 2019; Lee *et al.* 2020; Zhang *et al.* 2021), zebrafish Bcdin3 (Barboric *et al.* 2009), and *S. pombe* Bmc1
545 (Páez-Moscoso *et al.* 2022; Porat *et al.* 2022). We discovered a 16-amino acid motif that is almost
546 entirely conserved in metazoans (flies, zebrafish, and humans), but is absent in the fission yeast *S.*
547 *pombe* (**Fig. 4c**). Therefore, we have named this motif the Metazoan-Specific Motif (MSM). The N-
548 terminal portion of this motif is predicted to be more structured (IUPred3 score 0.2733 to 0.3764), while
549 the C-terminal portion is predicted to be less structured (IUPred3 score 0.4062 to 0.5887). Given the
550 strong conservation of the MSM, we hypothesized that the MSM must contribute to some important

551 function of Bin3 and its metazoan orthologs. To test this hypothesis, we used the Trojan GAL4 system
552 to generate flies expressing either Bin3^{wt} or Bin3 deleted of the entire 16-aa MSM (Bin3$^{\Delta MSM}$) and asked
553 whether Bin3$^{\Delta MSM}$ could (i) bind and stabilize 7SK, and (ii) rescue *bin3* mutant phenotypes.
554 We found that GAL4 expressed from *bin3*$^{TG4.0}$ induced both the *UAS-bin3*^{wt} (**Fig. 4h**) and *UAS-*
555 *bin3*$^{\Delta MSM}$ (**Fig. 4j**) transgenes to express similar levels of mRNA (P = .3840, **Fig. 4k**) and protein (P =
556 .7994, **Fig. 4l**). Given that the MSM is outside of the Bin3 methyltransferase domain, we did not expect
557 that the Bin3 MSM would be required for 7SK stability or binding. Accordingly, there was no significant
558 difference in 7SK levels (P = .3846, **Fig. 5a**) between Bin3$^{\Delta MSM}$ flies (*bin3*$^{TG4.0}$*/Df; UAS-bin3*$^{\Delta MSM}$/+) and
559 Bin3^{wt} flies (*bin3*$^{TG4.0}$*/Df; UAS-bin3*^{wt}/+). Also, Bin3$^{\Delta MSM}$ immunoprecipitated as much 7SK (P = .9938, **Fig.**
560 **5b**) as did Bin3^{wt}.
561 Given that 7SK was bound and stabilized by Bin3$^{\Delta MSM}$, we expected that Bin3$^{\Delta MSM}$ would rescue
562 the fecundity, climbing, and wing posture defects of *bin3*$^{TG4.0}$*/Df* flies. Indeed, Bin3$^{\Delta MSM}$ expression
563 rescued the fecundity (P = .0061, **Fig. 6a**) and climbing (P < .0001) defects of *bin3*$^{TG4.0}$*/Df* flies, similar to
564 Bin3^{wt} (P = .6681, **Fig. 6a**; P = .0685, **Fig. 6b**). However, Bin3$^{\Delta MSM}$ did not rescue the *held-out wings*
565 phenotype of *bin3*$^{TG4.0}$*/Df* flies (compare **Fig. 6g** with **Fig. 6d**), suggesting that while the MSM is
566 dispensable for Bin3 function in the contexts of egg-laying and climbing, the Bin3 MSM plays a critical
567 role in normal resting wing posture, independent of 7SK (**Fig. 6i**). Interestingly, reducing CycT dosage in
568 Bin3$^{\Delta MSM}$ flies (*bin3*$^{TG4.0}$*/Df; UAS-bin3*$^{\Delta MSM}$*/CycT*^{j11B2}) rescued the *held-out wings* defect (compare **Fig. 6h**
569 with **Fig. 6g**). We think that because Bin3$^{\Delta MSM}$ binds and stabilizes 7SK (and as such, forms the 7SK
570 snRNP to repress P-TEFb; **Fig. 5b**) it is unlikely that the MSM directly contributes to P-TEFb repression;
571 instead, genetically reducing P-TEFb activity probably had a non-specific rescuing effect by globally
572 tapering transcription elongation.
573
574 **Bin3 binds to the U6 spliceosomal RNA, but is not required for its stability**

MEPCE in humans (Jeronimo *et al.* 2007; Muniz *et al.* 2013) and Bmc1 in *S. pombe* (Páez-Moscoso *et al.* 2022; Porat *et al.* 2022) bind to the U6 spliceosomal snRNA, but are not required for U6 stability. We asked whether Bin3 in *Drosophila* also binds to U6 and whether Bin3 is also dispensable for U6 stability.

We found that $Bin3^{wt}$ (P = .0113), $Bin3^{Y795A}$ (P = .0033), and $Bin3^{\Delta MSM}$ (P = .0336) all bind to U6 snRNA, compared to un-tagged control. We also found that there is no significant difference in the amount of U6 bound by $Bin3^{Y795A}$ (P = .7671) or $Bin3^{\Delta MSM}$ (P = .8486) compared to $Bin3^{wt}$ (**Fig. 5d**). These results show for the first time that Bin3 in *Drosophila* binds to U6, and that neither catalytic activity nor the MSM are required for binding. It is not surprising that $Bin3^{\Delta MSM}$ binds to U6, as Bmc1 lacks this region (Cosgrove *et al.* 2012), yet it binds to U6 (Páez-Moscoso *et al.* 2022; Porat *et al.* 2022). And, like MEPCE and Bmc1, we found that Bin3 is not required for U6 stability. U6 levels (**Fig. 5c**) were not different between flies expressing $Bin3^{wt}$ and $Bin3^{Y795A}$ (P = .8794) or $Bin3^{\Delta MSM}$ (P = .7529), and were not significantly affected in $bin3^{2\text{-}7}/Df$ flies (P = .9314, **Fig. 1d**). U6 levels were reduced by approximately half in $bin3^{TG4.0}/Df$ flies (P = .0471, **Fig. 4g**); however, these data were just below the threshold for significance (α = 0.05). Taken together, Bmc1, Bin3, and MEPCE have a conserved function in binding to the U6 snRNA, but are not required for its stability.

DISCUSSION

In this study, we showed that Bin3, the *Drosophila* ortholog of the 7SK methylphosphate capping enzyme, MEPCE, has a conserved role in promoting normal metazoan development by regulating the P-TEFb positive elongation factor (**Figs. 7a, 8a**). We further investigated Bin3 by determining the *in vivo* requirement for two different regions of the Bin3 protein: the methyltransferase domain, and a previously undiscovered motif that is specific to metazoan orthologs of Bin3. To our surprise, we found that the catalytic activity of the methyltransferase domain appears to be dispensable for the function of Bin3 as a constituent of the repressive 7SK snRNP (**Fig. 7b**). By contrast, the metazoan-specific motif in Bin3 is required for a tissue-specific function, one that is 7SK-independent (**Figs. 7c, 8b**). We also provide the first evidence in *Drosophila* for binding of Bin3 to the U6 spliceosomal snRNA. As in other model organisms (Jeronimo *et al.* 2007; Muniz *et al.* 2013; Páez-Moscoso *et al.* 2022; Porat *et al.* 2022), we found that Bin3 was not required for U6 stability.

Bin3 represses P-TEFb to promote normal fly physiology

The canonical function of MEPCE is to *repress* gene expression by binding to and stabilizing 7SK snRNA, which acts as a scaffold for proteins that sequester P-TEFb (Peterlin *et al.* 2011; Cosgrove *et al.* 2012). This inhibits P-TEFb, which normally phosphorylates RNAPII to promote transcription elongation. Consequently, loss of MEPCE function destabilizes 7SK, dissociates the repressive snRNP, releasing P-TEFb (Fujinaga *et al.* 2023). Hyper-activated P-TEFb induces aberrant gene expression by ectopic phosphorylation of RNAPII and other factors (He *et al.* 2008; Schneeberger *et al.* 2019). A non-canonical function of MEPCE is to *activate* gene expression by binding to the tail of histone H4 and recruiting free P-TEFb to chromatin. This non-canonical function was found be required for the induction of tumorigenic genes in a breast cancer cell line (Shelton *et al.* 2018). Here, we show that Bin3 contributes to normal fly physiology through a mechanism most consistent with its canonical function

in repression of P-TEFb. We found that the egg-laying, climbing, and wing posture defects of *bin3* mutants were rescued by genetically reducing the activity of P-TEFb with a mutation in *CycT* (which is needed for P-TEFb kinase activity). Thus, in fly development, Bin3 appears to repress P-TEFb (and gene expression) rather than to activate P-TEFb (**Figs. 7a, 8a**).

Bin3 is required for reproductive success

Previously, we found that Bin3 plays a role in fertility by promoting embryonic viability (Singh *et al.* 2011). Here, we show that Bin3 is required for fecundity by supporting a normal egg-laying rate (**Fig. 7a**). Thus, Bin3 has a role in two different aspects of reproductive success: fertility (offspring viability), and fecundity (the rate of offspring production).

Although Bin3 and its substrate 7SK are expressed in all germline and somatic cells of the ovary, germline expression of Bin3 was dispensable for a normal egg-laying rate. A germline function for Bin3 might occur later in development, consistent with our previous finding that Bin3 appears to regulate the translation of *grk* in late-stage oocytes (Singh *et al.* 2011), which is important for embryonic patterning.

A previous report demonstrated that both wild-caught flies harboring indels in *bin3*, and transgenic flies harboring transposon insertions into *bin3*, have reduced numbers of ovarioles (Lobell *et al.* 2017). However, we found that our $bin3^{2-7}/Df$ mutant females did not exhibit reduced ovariole numbers compared to controls. We suggest that the difference between our findings and those of Lobell *et al.* (2017) might be attributable to differences in genetic backgrounds. Nevertheless, the wild-type number of ovarioles established in our *bin3* mutants is not sufficient to promote a normal egg-laying rate. Egg-laying is in part a neuromuscular process, as muscle contractions of the ovary and uterus promote successful oviposition (i.e., egg-laying; Deady and Sun 2015; Irizarry and Stathopoulos 2015; Liao and Nässel 2020; Garrett *et al.* 2023). It is possible, therefore, that defects in neuromuscular

638 function that we observe in *bin3* mutants (see below) might also explain why *bin3* mutant females lay
639 fewer eggs, *e.g.*, due to a reduction in the frequency or strength of these contractions.
640
641 **Conserved role of Bin3 and MEPCE in metazoan neurodevelopment**
642 A patient with a neurodevelopmental disorder characterized by mobility and musculature
643 deficiencies was shown to carry a heterozygous nonsense mutation in *MEPCE* (Schneeberger *et al.*
644 2019). Similarly, we found that *bin3* mutant flies exhibited difficulties in climbing and an inability to
645 properly fold their wings, phenotypes that are characteristic of neuromuscular defects (Shukla *et al.*
646 2013; Kairamkonda and Nongthomba 2014; Sanhueza *et al.* 2014; Manjila and Hasan 2018). Many
647 mutations in *Drosophila* can affect wing posture (see below), including those in the highly-conserved
648 JAK/STAT pathway (Harrison *et al.* 1998; Callus and Mathey-Prevot 2002; Ayala-Camargo *et al.* 2013;
649 Hatini *et al.* 2013; Johnstone *et al.* 2013). Therefore, the conserved roles of Bin3 and MEPCE in
650 metazoan neurodevelopment may occur through the JAK/STAT pathway. While the exact mechanisms
651 remain to be determined, the phenotypes we observe in *bin3* mutants (egg-laying, climbing, wing
652 posture) can be attributable to neuromuscular defects, suggesting a strong conservation in the
653 developmental function of Bin3 and MePCE in *Drosophila* and human development.
654 Bin3/MEPCE methylates the gamma phosphate on the 5′ end of the 7SK snRNA, while another
655 class of RNA methyltransferases methylates the N^6 position of internal adenosines (N^6-
656 methyladenosine, m^6A) on "RRACH" motifs (Wang *et al.* 2018) in a variety of RNAs (Lence *et al.* 2018).
657 Interestingly, both human 7SK (Warda *et al.* 2017; Leger *et al.* 2021; Perez-Pepe *et al.* 2023) and mouse
658 7SK (Xu *et al.* 2022) contain the m^6A modification. In HeLa cells, methylation of 7SK by the METLL3
659 m^6A "writer" protein in response to EGF signaling allows hnRNPs to associate with 7SK; this causes
660 HEXIM to dissociate from the 7SK snRNP and release P-TEFb, which activates transcriptional
661 elongation (Perez-Pepe *et al.* 2023). In mice, methylation of 7SK at adenine 281 by METLL3 is required

662 for the binding of m^6A "reader" proteins to establish proper 7SK secondary structure (Xu *et al.* 2022).
663 *Drosophila* 7SK contains a single RRACH motif at position 397-401; however, it is not known whether
664 the adenine within this motif is methylated, or if m^6A at that position would serve functions similar to
665 those in HeLa cells or mice. Intriguingly, flies mutant for m^6A writers (and m^6A readers) exhibit the
666 same neuromuscular defects in both climbing and resting wing posture (Lence *et al.* 2016; Kan *et al.*
667 2017) as flies mutant for *bin3* (this study). Therefore, it is possible that *Drosophila* 7SK might also
668 contain the m^6A modification (at A399), and that m^6A is important for 7SK stability and function in
669 neurodevelopmental processes in *Drosophila*.

670 Although Bin3 and the m^6A pathway might function synergistically to promote 7SK stability and
671 function, they seem to act antagonistically on transcription elongation: Bin3 is required to *prevent*
672 RNAPII pause-release, whereas the m^6A pathway has been shown in *Drosophila* to *promote* RNAPII
673 pause-release (Akhtar *et al.* 2021). Clearly, there is a complex balance between 7SK stability (via Bin3
674 binding and possible m^6A methylation) as well as 7SK functions that sequester P-TEFb (Bin3-mediated
675 function) or release P-TEFb (m^6A modification function) that is governed by the activities of diverse
676 classes of RNA methyltransferases, which in *Drosophila* contribute to neuromuscular function.
677 Moreover, it appears that m6A modifications in 7SK might serve species-specific roles in 7SK biology.

678 Neuromuscular disorders arise from developmental defects in motoneurons and/or the muscles
679 that they control. We attempted to identify the cells and tissues that require Bin3 for neuromuscular
680 function by performing an RNAi screen using over 90 GAL4 drivers active in specific neuron and muscle
681 cell types that drive the expression of two different short hairpin RNAs (shRNAs) targeting *bin3* coding
682 sequence (Ni *et al.* 2011). However, we did not identify any conditions under which *bin3* RNAi
683 knockdown recapitulated the neuromuscular phenotypes of *bin3* mutant flies. The failure of our screen
684 might be due to technical reasons such as weak GAL4 drivers and/or insufficient levels of RNAi
685 knockdown, or they could be due to Bin3 being required in more than one tissue simultaneously for

686 neuromuscular activity. Indeed, knockdown of *bin3* induced by the Trojan-GAL4 *bin3* allele (which also
687 functions as a null allele) in the spatiotemporal expression pattern of *bin3* recapitulated the *held-out*
688 *wings* phenotype of *bin3* mutant flies (data not shown), suggesting that Bin3 might be required in
689 multiple cell types simultaneously, at least for normal resting wing posture.
690
691 **Bin3 catalytic activity is dispensable for 7SK stability and snRNP function *in vivo***
692 MEPCE modifies the 5′ end of 7SK RNA by catalyzing the addition of a monomethyl cap to the
693 gamma phosphate (Gupta *et al.* 1990b; Shumyatsky *et al.* 1990; Jeronimo *et al.* 2007; Xue *et al.* 2010;
694 Yang *et al.* 2019). It has long been thought that the monomethyl cap is essential for 7SK stability. For
695 example, *in vitro* transcribed capped 7SK was more stable than uncapped 7SK when injected into
696 *Xenopus* oocytes (Shumyatsky *et al.* 1993). However, whether 7SK requires a monomethyl cap for
697 stability *in vivo* has never been adequately addressed. We and others have shown that Bin3 and its
698 orthologs are essential for 7SK stability, as deletion of *bin3* (Singh *et al.* 2011), siRNA-mediated
699 knockdown of *MEPCE* in human cells (Jeronimo *et al.* 2007; Xue *et al.* 2010), and morpholino-mediated
700 disruption of *mepcea* splicing in zebrafish embryos (Barboric *et al.* 2009) reduces 7SK levels.
701 Importantly, these approaches do not explicitly test the *in vivo* requirement for methyltransferase
702 activity, which requires the use of catalytic mutants.
703 Catalytic mutants of MEPCE have been characterized *in vitro*. A triple mutation in the active site
704 (V447A, L448A, and D449A) abolished methyltransferase activity, likely by preventing the interaction
705 between MEPCE and the methyl donor *S*-adenosyl-methionine (SAM). However, this mutant is also
706 defective for binding to 7SK and therefore it is not a catalytic mutant *per se* (Xue *et al.* 2010). A double
707 mutant in the active site (G451A and G455A) also abolished MEPCE methyltransferase activity, again,
708 presumably by preventing the interaction between MEPCE and SAM; however, this mutant does bind
709 to 7SK (Shelton *et al.* 2018). Finally, a single amino acid mutation in the active site (Y421A) reduced

methyltransferase activity to 0.6% that of the wt enzyme. This is likely due to loss of hydrogen bonds between Y421 and both an adjacent residue (R425) and the 7SK gamma phosphate, which is the recipient of the methyl group from SAM (Yang *et al.* 2019). Importantly, Y421A is not expected to disrupt binding to either the methyl donor co-factor or the RNA substrate, but rather to disrupt the chemistry of methyl transfer to the gamma phosphate (Yang *et al.* 2022). Therefore, given the precise and specific nature of this active site mutation, our preferred choice for *in vivo* study of the importance of methyl capping was a Y795A substitution in Bin3 (orthologous to Y421A in MEPCE).

Unexpectedly, we found that the Bin3^{Y795A} mutant did not exhibit any of the physiological defects exhibited by *bin3* deletion mutants, suggesting that catalytic activity is not required for Bin3 function *in vivo* (**Fig. 8a**). This result could be explained, in part, by our finding that Bin3^{Y795A} still bound and stabilized 7SK no differently than Bin3^{wt}, despite its expected lack of methyltransferase activity (**Fig. 7b**). Thus, flies expressing the Bin3^{Y795A} allele retain the ability to assemble the 7SK snRNP to repress P-TEFb and promote normal development. Our findings suggest that *in vivo* capping of endogenous 7SK is not required for its stability *per se*, so long as Bin3 is able to bind to 7SK.

That the Bin3^{Y795A} catalytic mutant protein was still able to bind to 7SK is not entirely surprising. Y421 in MEPCE (analogous to Y795 in Bin3) is located within a disordered region that becomes ordered upon binding to 7SK, forming an alpha helix (Yang *et al.* 2022); this disorder-to-order transition is required for MEPCE methyltransferase activity. When LARP7 binds to 7SK and then associates with MEPCE, the alpha helix containing Y421 becomes disordered again (Yang *et al.* 2022); this order-to-disorder transition induced by LARP7 binding inhibits MEPCE methyltransferase activity (Xue *et al.* 2010; Brogie and Price 2017; Yang *et al.* 2022). Therefore, MEPCE bound by LARP7 effectively phenocopies MEPCE with a Y421A mutation, which is catalytically-dead (Yang *et al.* 2019). Thus, it appears that Y421 in MEPCE and Y795 in Bin3 are not essential for 7SK binding, but instead are essential only for methyl capping.

Our finding that the Bin3^{Y795A} catalytic mutant protein not only bound 7SK, but stabilized 7SK despite the expected lack of catalytic activity, suggests that RNA binding contributes more to 7SK stability than does methyl capping, challenging the assumption that the gamma monomethyl cap is essential for 7SK stability. This is underscored by the fact that U6 snRNA, which binds to and is presumed to be capped by Bin3 and its orthologs, is stable in the absence of these proteins (Jeronimo *et al.* 2007; Muniz *et al.* 2013; Páez-Moscoso *et al.* 2022; Porat *et al.* 2022).

Bin3 and its orthologs are peculiar enzymes, in that they remain associated with the products of the reaction they catalyze (Xue *et al.* 2010; Yang *et al.* 2019, 2022). MEPCE has a higher affinity both for capped 7SK and SAH (the products) than uncapped 7SK and SAM (the reactants) (Yang *et al.* 2019). Therefore, the gamma monomethyl cap might be required not for 7SK stability *per se*, but to enhance the binding of MEPCE to the 5′ end of 7SK to keep the enzyme bound after catalyzing the methyltransferase reaction. Constitutive binding of MEPCE to 7SK would serve the dual purposes of physically protecting 7SK from inorganic phosphatases (for which the gamma monomethyl cap is a substrate; Shumyatsky *et al.* 1990), and aiding in the recruitment of LARP7, which binds weakly to 7SK in the absence of MEPCE (Xue *et al.* 2010), but enhances the affinity of MEPCE for 7SK after binding (Muniz *et al.* 2013; Yang *et al.* 2022). However, our finding that the Bin3^{Y795A} catalytic mutant bound as much 7SK as Bin3^{wt} despite the lack of a gamma monomethyl cap is not consistent with such a model (at least not *in vivo*). Instead, our results support a model in which 7SK RNA secondary structure—and not the gamma monomethyl cap—is required for Bin3 and its orthologs to bind to 7SK. Indeed, MEPCE bound equally well to transfected 7SK harboring either the normal gamma monomethyl cap or a tri-methyl guanosine (TMG) cap (Muniz *et al.* 2013), and Bmc1 (the *S. pombe* ortholog of Bin3) binds to both gamma monomethyl-capped U6 RNA and TMG-capped telomerase RNA (Páez-Moscoso *et al.* 2022; Porat *et al.* 2022). These findings suggest that a gamma monomethyl cap structure is not specifically required for constitutive or high-affinity binding by MEPCE and its orthologs. Alternatively,

758 7SK secondary structure features likely mediate initial association with MEPCE (i.e., prior to the
759 association of LARP7, which enhances the affinity of MEPCE for 7SK). When MEPCE initially binds to
760 7SK in the "nascent" conformation (adopted during 7SK synthesis), there is extensive hydrogen
761 bonding between the methyltransferase domain and the 5′ hairpin of 7SK (Yang *et al.* 2019). Binding of
762 MEPCE to 7SK requires the first two (Singh *et al.* 1990) to three (Muniz *et al.* 2013) base pairs of the 5′
763 hairpin, and a portion of the single-stranded DNA 3′ to the hairpin (Shumyatsky *et al.* 1994; Muniz *et al.*
764 2013; Yang *et al.* 2019). Subsequently, LARP7 binds to the complex of MEPCE and 7SK, and the
765 conformation of 7SK changes from a "nascent" conformation to a "closed" conformation (adopted after
766 formation of the core snRNP of MEPCE, 7SK, and LARP7). In this conformation, MEPCE forms
767 additional hydrogen bonds to 7SK, and thereby has higher affinity for the "closed" conformation of 7SK
768 than for the "nascent" conformation of 7SK (Yang *et al.* 2022). Therefore, both 7SK secondary structure
769 and association with LARP7 are likely the major contributors to the constitutive binding of MEPCE to
770 7SK.

771 One possible circumstance under which the gamma monomethyl cap on 7SK might be essential
772 for stability is when the 7SK snRNP is actively repressing P-TEFb. For HEXIM to bind to 7SK and
773 sequester P-TEFb, 7SK must undergo a conformational change from the "closed" conformation (i.e.,
774 the "core" snRNP conformation) to the "linear" conformation (i.e., the "repressive" snRNP
775 conformation). In this conformation, the 5′ end of 7SK is located outside of the MEPCE active site (Yang
776 *et al.* 2022), and therefore, in the context of the repressive 7SK snRNP, the 5′ end of 7SK might be
777 solvent-exposed, which would necessitate a gamma monomethyl cap to protect 7SK from
778 exoribonucleolytic degradation. However, these findings are based on crystal structures using a
779 recombinant MEPCE comprising only the methyltransferase domain. Our finding that 7SK is not only
780 bound but is also stabilized by $Bin3^{Y795A}$ catalytic mutant protein (just like $Bin3^{wt}$ protein) leaves open
781 the possibility that there are regions outside of the methyltransferase domain in full-length

Bin3/MEPCE that protects the 5′ end of 7SK, even when located outside of the active site. Moreover, the finding that the 5′ end of 7SK might not be bound by MEPCE when in the "linear" conformation further supports a model in which the gamma monomethyl cap is not required for constitutive binding of MEPCE to 7SK.

If the monomethyl cap is not required for either 7SK stability or for Bin3 binding, then what is the purpose of the methyltransferase domain in Bin3 and its orthologs? One possibility is that the methyltransferase domain is a vestige of an ancestral ortholog of Bin3 that did not remain constitutively bound to its RNA substrates, and therefore, the monomethyl cap would have been essential to protect these RNAs from 5′-3′ exoribonucleolytic degradation. The acquisition of additional protein binding constituents during evolution of a primordial 7SK snRNP complex might have necessitated that Bin3 remain associated with 7SK (after catalyzing the methyltransferase reaction) to facilitate the stable interaction of these additional components (like Larp7). This process would have rendered the monomethyl capping reaction dispensable for 7SK stability, as we observe. A second possibility, supported by the strong conservation of the methyltransferase domain over evolutionary time, argues that catalytic activity has an important function that has yet to be identified, perhaps on substrates other than 7SK.

A metazoan-specific motif in Bin3 facilitates a 7SK-independent, tissue-specific function in neurodevelopment

S. pombe Bmc1, the most ancient ortholog of Bin3 studied to date, consists only of the conserved methyltransferase domain (Cosgrove *et al.* 2012; Páez-Moscoso *et al.* 2022; Porat *et al.* 2022). Over the course of evolution, Bin3 orthologs gained additional protein sequence flanking the methyltransferase domain (Cosgrove *et al.* 2012). We found a 16-amino acid motif N-terminal to the methyltransferase domain that is highly conserved in metazoans, and is mostly unstructured. Given its

location outside of the methyltransferase domain, we were not surprised to find that this metazoan-specific motif (MSM) was not required for Bin3 to bind or stabilize 7SK *in vivo*, and consequently, was dispensable for fecundity and climbing ability. What we did not expect, however, was that flies expressing Bin3 deleted of the MSM (Bin3$^{\Delta MSM}$) were unable to properly fold their wings, phenocopying *bin3* null mutants (**Fig. 7c**). These findings suggest that the Bin3 MSM plays a tissue-specific role in gene regulation independent of 7SK (**Fig. 8b**). There is likely one or more MSM-interacting proteins that help Bin3 regulate gene expression. These proteins might be specifically expressed in the tissues involved in wing posture (*e.g.*, the direct and indirect flight muscles), or they might be ubiquitously expressed, but the interaction with the Bin3 MSM is essential for Bin3 function only in tissues contributing to normal resting wing posture. Moreover, this protein might be incorporated into the core snRNP of 7SK, Bin3, and Larp7 to generate a novel 7SK snRNP, or the association with Bin3 MSM might be independent of the 7SK snRNP altogether.

A 7SK-independent function of Bin3 is not without precedent. It was previously shown that fibroblasts from a patient with a nonsense mutation in *MEPCE* (*MEPCE* haploinsufficient cells) and cells deleted of *LARP7* (*LARP7* KO cells) both had reduced levels of 7SK, as expected, but that genes up-regulated in *MEPCE* haploinsufficient cells were not affected in *LARP7* KO cells. Moreover, exogenous *MEPCE* rescued the up-regulation phenotype of *MEPCE* haploinsufficient cells, despite only leading to a small increase in 7SK levels. Based on these findings, Schneeberger *et al.* (2019) hypothesized that MEPCE might have a 7SK-independent role in regulating transcription, potentially by interacting with as-yet unknown proteins. Our finding that Bin3$^{\Delta MSM}$ binds and stabilizes 7SK but is not sufficient to rescue all *bin3* mutant phenotypes supports this hypothesis and suggests that the as-yet unknown proteins that interact with Bin3/MEPCE to regulate transcription does so through the MSM, independent of the 7SK snRNP.

Conclusions

In summary, we have carried out the first detailed *in vivo* study of the highly-conserved Bin3/MEPCE RNA methyltransferase in a metazoan host. The surprising results demonstrate the value of rigorously testing models for enzyme function in whole organisms. Our study establishes *Drosophila* as a genetically tractable developmental model for further dissection of Bin3/MEPCE and 7SK non-coding RNA pathways, and how their disruption may be associated with human disease.

DATA AVAILABILITY

Plasmids and *Drosophila* stocks are available upon request. All reagent inquiries should be directed to RJP. All data required to confirm the conclusions made in this article are presented in the text, figures, and tables.

ACKNOWLEDGEMENTS

We are grateful to the Bloomington *Drosophila* Stock Center (NIH Grant P40OD018537) for fly stocks, the *Drosophila* Genomics Resource Center (NIH Grant 2P40OD010949) for plasmid pUASP-attB; Jian-Quan Ni for plasmid pNP; BestGene, Inc. for generating transgenic flies; and David Price for anti-CycT antiserum. We are also grateful to Scott Neal, Mark Bayfield, and Jennifer Porat for helpful discussions.

FUNDING

This work and RJP was supported by grants to S. Hanes (NSF MCB-1515076 and NIH R-01 GM123985-01) and B. Knutson (NIGMS R01-GM141033).

CONFLICTS OF INTEREST

None declared.

853 **FIGURE LEGENDS**

854 **Figure 1. Molecular characterization of *bin3* mutant and rescue flies. (a)** Graphic depicting the ~26 kb
855 *bin3* locus on chromosome 2R (cytogenetic bands 42A13-42A14). Two promoters, P1 and P2 (grey),
856 drive expression of *bin3* (Zhu and Hanes 2000; Singh *et al.* 2011). The *bin3* ORF (salmon) comprises 6
857 coding exons. $bin3^{\Delta}$ refers to the $bin3^{2\text{-}7}$ excision allele created by FLP/FRT-mediated recombination
858 between transposon insertions $PBac\{RB\}bin3^{e02231}$ and *P{XP}d02161* (Parks *et al.* 2004; Singh *et al.* 2011).
859 *Df* refers to deficiency *Df(2R)ED1612*, which deletes ~829 kb of chromosome 2R, including promoter P1
860 and all *bin3* coding sequence (Ryder *et al.* 2004). $bin3^{\Delta}$ and *Df* in *trans* produce *bin3* mutant flies. $bin3^{+}$
861 (sky blue) is a transgenic insertion of a BAC comprising ~20 kb of chromosome 2R, including promoter
862 P1 and all *bin3* coding sequence. In $bin3^{2\text{-}7}/Df$ flies, this insertion rescues *bin3* mutant phenotypes. **(b-d)**
863 Bar graphs showing the average amount of *bin3* mRNA (b), 7SK snRNA (c), and U6 snRNA (d) in total
864 RNA extracted from ovaries of females of the indicated genotypes, for three biological replicates. Note
865 that *bin3* mRNA was below the level of detection in $bin3^{2\text{-}7}/Df$ and $bin3^{2\text{-}7}/Df;\ CycT^{j11B2}/+$ ovaries for 2 of
866 the three biological replicates. RNA levels were normalized to *rp49* mRNA and made relative to wt
867 using CFX Maestro 2.0 (version 5.2.008.0222, Bio-Rad). Error bars represent the standard error of the
868 mean. Statistical significance was calculated by unpaired t-test using CFX Maestro 2.0 (version
869 5.2.008.0222, Bio-Rad). *P* values of <.05 (*), <0.001 (***), <.0001 (****), and not significant (ns) are
870 indicated. **(e)** Western blot for CycT (Nguyen *et al.* 2012) and Actin in extracts prepared from ovaries of
871 females of the indicated genotypes. The $P\{lacW\}j11B2^{j11B2}$ insertion (Spradling *et al.* 1999) into one of the
872 two different *CycT* 5′-UTRs reduces expression of the large isoform of CycT.

873

874 **Figure 2. Bin3 is ubiquitously expressed in the ovary and is required for egg-laying, but is not**
875 **required to establish ovarioles and does not function in germline to promote egg-laying. (a)** Scatter
876 plot showing the egg-laying rates of females of the indicated genotypes for each of three biological

replicates. Error bars represent the standard deviation. Statistical significance compared to *bin3*$^{2-7}$*/Df* was calculated by nested one-way ANOVA with Dunnett's Correction for multiple comparisons, using Prism (version 9.4.1, GraphPad). *P* values of <.001 (***) and <.0001 (****) are indicated. **(b)** Cartoon depicting a single ovariole, of which 16-20 make up a single adult ovary. Germline cells are indicated in pink, nurse cell nuclei (arrow) are indicated in purple, oocytes are indicated in blue, and somatic cells surrounding the germline and oocytes are indicated in purple. **(c to d')** Immunofluorescence staining of adult ovaries for 3xHA-Bin3 (green), Vasa (a cytoplasmic marker for germline cells; blue), and Hoechst staining of DNA (red). Scale bars = 100 µm. A Trojan-GAL4 phase 0 insertion in *bin3* (*bin3*$^{TG4.0}$) was used to drive expression of a *UAS-3xHA-bin3* transgene in the pattern of *bin3* expression (*bin3*$^{TG4.0}$ > *UAS-bin3-3xHA*). 3xHA-Bin3 localizes to the nuclei of all germline and somatic cells (C-C'). No HA staining was detected in *bin3*$^{TG4.0}$ control ovaries (D-D'), demonstrating the specificity of HA staining in *bin3*$^{TG4.0}$ > *UAS-3xHA-bin3* ovaries. **(e-f')** Single-molecule fluorescence *in situ* hybridization (smFISH) of adult ovaries for 7SK (green) and Hoechst staining of DNA (purple). Scale bars = 100 µm. 7SK localizes to the nuclei of all germline and somatic cells in wt ovaries (E-E'). 7SK staining is absent in *bin3*$^{2-7}$*/Df* ovaries (F-F'), which do not accumulate 7SK (see Fig. 1c). **(g)** Scatter plot showing the mean number of ovarioles per ovary per female of the indicated genotypes for each of two biological replicates. Error bars represent the standard deviation. Statistical significance compared to *bin3*$^{2-7}$*/Df* was calculated by nested one-way ANOVA with Dunnett's Correction for multiple comparisons, using Prism (version 9.4.1, GraphPad). *P* values of not significant (ns) are indicated. **(h)** Scatter plot showing the absolute value of the difference between ovariole number within a pair of ovaries per female of the indicated genotypes for each of two biological replicates. Error bars represent the standard deviation. Statistical significance compared to *bin3*$^{2-7}$*/Df* was calculated by nested one-way ANOVA with Dunnett's Correction for multiple comparisons, using Prism (version 9.4.1, GraphPad). *P* values of not significant (ns) are indicated. **(i)** Scatter plot showing the egg-laying rates of females of the indicated genotypes

901 for each of three biological replicates. Error bars represent the standard deviation. Statistical
902 significance compared to *bin3*$^{2-7}$*/Df; nanos-GAL4::VP16/+* was calculated by nested one-way ANOVA
903 with Dunnett's Correction for multiple comparisons, using Prism (version 9.4.1, GraphPad). *P* values of
904 <.05 (*), <.001 (***) and not significant (ns) are indicated.
905
906 **Figure 3. Bin3 is required for neuromuscular function.** (**a**) Scatter plot showing the percent of flies of
907 the indicated genotypes climbing 8 cm in 12" in each of 10 trials, for each of three biological replicates.
908 Error bars represent the standard deviation. Statistical significance compared to *bin3*$^{2-7}$*/Df* was
909 calculated by nested one-way ANOVA with Dunnett's Correction for multiple comparisons, using Prism
910 (version 9.4.1, GraphPad). *P* value of <.001 (***) is indicated. (**b-e**) Images of females of the indicated
911 genotypes, exhibiting either a normal resting wing posture or a *held-out wings* phenotype. (**f**) Scatter
912 plot showing the percent of flies of the indicated genotypes climbing 8 cm in 12" in each of 4 trials, for
913 each of three biological replicates. Error bars represent the standard deviation. Statistical significance
914 was calculated by nested t-test, using Prism (version 9.4.1, GraphPad). *P* value of not significant (ns) is
915 indicated. (**g-h**) Images of females of the indicated genotypes, exhibiting either a normal resting wing
916 posture or a *held-out wings* phenotype.
917
918 **Figure 4. Molecular characterization of the *bin3*$^{TG4.0}$ Trojan GAL4 allele and Bin3 protein mutants.**
919 (**a**) Bin3 modeled onto the crystal structure of 309 amino acids of the MEPCE active site (Yang *et al.*
920 2019). Y421 in MEPCE (black) is juxtaposed between the 7SK 5′ gamma phosphate (orange and salmon)
921 and *S*-adenosyl-homocysteine (SAH, blue and gold), and is essential for MEPCE catalytic activity *in vitro*
922 (Yang *et al.* 2019). Y795 in Bin3 (red) aligns with Y421 in MEPCE (RMSD = 0.000). (**b**) Same as in (a), but
923 with the Y421A (MEPCE, black) and Y795A (Bin3, red) tyrosine-to-alanine mutations introduced. Y421A
924 completely eliminated MEPCE catalytic activity *in vitro* (Yang *et al.* 2019). (**c**) Partial alignment of Bin3

925 orthologs from *D. melanogaster*, *H. sapiens* (MEPCE), *D. rerio* (BCDIN3), and *S. pombe* (Bmc1).
926 Conserved residues are in boldface. **(d)** Graphic depicting the *bin3* locus, as in **Fig. 1a**. *bin3*$^{TG4.0}$ refers to
927 a transgenic insertion of a Trojan GAL4 phase 0 (TG4.0) construct into the second intron in the *bin3* ORF
928 (Lee *et al.* 2018). A splice acceptor (SA) in the insertion causes the TG4.0 cassette to be spliced into the
929 *bin3* mRNA; transcription is terminated at the end of the cassette by a synthetic poly(A) sequence.
930 When the chimeric *bin3*$^{TG4.0}$ mRNA is translated, T2A, a viral peptide sequence, disrupts translation and
931 causes the release of the nonfunctional Bin3:T2A chimeric peptide from the ribosome; subsequently,
932 the ribosome resumes translation of full-length GAL4 protein. *Df* refers to deficiency *Df(2R)BSC313*,
933 which deletes ~625 kb of chromosome 2R, including promoters P2 and P1, and all *bin3* coding sequence
934 (Cook *et al.* 2012). *bin3*$^{TG4.0}$ and *Df* in *trans* produce *bin3* mutant flies that express *GAL4* in the pattern of
935 *bin3* expression. GAL4 then binds to UAS and drives expression of *UAS-bin3* transgenes (see **Fig. 4h-j**).
936 **(e-g)** Bar graphs showing the average amount of *bin3* mRNA (e), 7SK snRNA (f), and U6 snRNA (g) in
937 total RNA extracted from ovaries of females of the indicated genotypes, for three biological replicates.
938 RNA levels were normalized to *rp49* mRNA and made relative to wt using CFX Maestro 2.0 (version
939 5.2.008.0222, Bio-Rad). Error bars represent the standard error of the mean. Statistical significance was
940 calculated by unpaired t-test using CFX Maestro 2.0 (version 5.2.008.0222, Bio-Rad). *P* values of <.05
941 (*), <0.01 (**), <.0001 (****), and not significant (ns) are indicated. **(h-j)** Graphic depicting *UAS-DSCP-*
942 *3xHA-bin3* transgenes. UAS-DSCP (grey) is a GAL4-responsive promoter that is active in both germline
943 and somatic cells (Pfeiffer *et al.* 2008). *bin3* cDNAs encode Bin3 proteins that are either wt (h; sky blue),
944 catalytically-dead (I; Y795A, pink), or deleted of the MSM (j; ΔMSM, maroon). Each construct is tagged
945 at the C-terminus with 3xHA that is codon-optimized for *Drosophila* (green). When these transgenes are
946 independently crossed into the *bin3*$^{TG4.0}$*/Df* background (see **Fig. 4d**), flies will express only 3xHA-Bin3,
947 3xHA-Bin3^{Y795A}, or 3xHA-Bin3$^{\Delta MSM}$ proteins, respectively. **(k)** Bar graph showing the average amount of
948 *bin3* mRNA in total RNA extracted from ovaries of females of the indicated genotypes, for three

biological replicates. RNA levels were normalized to *rp49* mRNA and made relative to *bin3*$^{TG4.0}$*/Df; UAS-bin3/+* using CFX Maestro 2.0 (version 5.2.008.0222, Bio-Rad). Error bars represent the standard error of the mean. Statistical significance was calculated by unpaired t-test using CFX Maestro 2.0 software (version 5.2.008.0222, Bio-Rad). *P* value of not significant (ns) is indicated. All three *UAS-bin3* transgenes are expressed to similar levels. **(i)** Representative Western blot for 3xHA-Bin3 proteins and Actin in extracts prepared from ovaries of females of the indicated genotypes. The relative amounts of 3xHA-Bin3^{Y795A} and 3xHA-Bin3$^{\Delta MSM}$ relative to 3xHA-Bin3 (wt) ± the standard deviation from two biological replicates are indicated below. Statistical significance was calculated by ordinary one-way ANOVA with Dunnett's Correction for multiple comparisons with a single pooled variance, using Prism (version 9.4.1, GraphPad). *P* values of <0.05 (*) and not significant (ns) are indicated. All three transgenes produce similar amounts of 3xHA-Bin3 proteins.

Figure 5. Neither catalytic activity nor the metazoan-specific motif are required for 7SK or U6 binding and stability. **(a** and **c)** Bar graphs showing the average amount of 7SK (a) and U6 (c) RNAs in total RNA extracted from ovaries of females of the indicated genotypes, for three biological replicates. RNA levels were normalized to *rp49* mRNA and made relative to *bin3*$^{TG4.0}$*/Df; UAS-bin3/+* using CFX Maestro 2.0 (version 5.2.008.0222, Bio-Rad). Error bars represent the standard error of the mean. Statistical significance was calculated by unpaired t-test using CFX Maestro 2.0 (version 5.2.008.0222, Bio-Rad). *P* value of not significant (ns) is indicated. **(b** and **d)** Bar graphs showing the average amount of 7SK (b) and U6 (d) RNA bound by 3xHA-Bin3 proteins immunoprecipitated with anti-HA magnetic beads from extracts prepared from ovaries of females of the indicated genotypes, for three biological replicates. The ratio of immunoprecipitated RNA to input RNA, from flies expressing 3xHA-Bin3 proteins relative to flies not expressing 3xHA-Bin3 proteins (*bin3*$^{TG4.0}$/+), was calculated using CFX Maestro 2.0 (version 5.2.008.0222, Bio-Rad). Error bars represent the standard error of the mean.

973 Statistical significance compared to *bin3*$^{TG4.0}$/+ (black asterisks) or *bin3*$^{TG4.0}$*/Df; UAS-bin3*/+ (sky blue
974 asterisks) was calculated by one-way ANOVA with Benjamini-Hochberg correction for false discovery
975 rate, using CFX Maestro 2.0 (version 5.2.008.0222, Bio-Rad). *P* values of <0.05 (*), <.01 (**), <.0001
976 (****), and not significant (ns) are indicated.
977
978 **Figure 6. Phenotypic characterization of Bin3^{Y795A} and Bin3$^{\Delta MSM}$ mutant proteins *in vivo*.** (**a**) Scatter
979 plot showing egg-laying rates of females of the indicated genotypes for each of three biological
980 replicates. Error bars represent the standard deviation. Statistical significance compared to *bin3*$^{TG4.0}$*/Df*
981 (salmon asterisks) or *bin3*$^{TG4.0}$*/Df; UAS-bin3*/+ (sky blue asterisks) was calculated by nested one-way
982 ANOVA with Dunnett's Correction for multiple comparisons, using Prism (version 9.4.1, GraphPad). *P*
983 values of <.01 (**), <0.001 (***), <.0001 (****), and not significant (ns) are indicated. (**b**) Scatter plot
984 showing the percent of flies of the indicated genotypes climbing 8 cm in 12" in each of 10 trials, for each
985 of three biological replicates. Error bars represent the standard deviation. Statistical significance
986 compared to *bin3*$^{TG4.0}$*/Df* (salmon asterisks) or *bin3*$^{TG4.0}$*/Df; UAS-bin3*/+ (sky blue asterisks) was calculated
987 by nested one-way ANOVA with Dunnett's Correction for multiple comparisons, using Prism (version
988 9.4.1, GraphPad). *P* values of <.0001 (****) and not significant (ns) are indicated. (**c-h**) Images of
989 females of the indicated genotypes, exhibiting either a normal resting wing posture or a *held-out wings*
990 phenotype.
991
992 **Figure 7. Summary of Bin3^{wt}, Bin3^{Y795A}, and Bin3$^{\Delta MSM}$ protein functions.** (**a**) Bin3^{wt} binds, caps, and
993 stabilizes 7SK, which allows for P-TEFb to be sequestered and repressed, which prevents RNAPII pause-
994 release and promotes egg-laying, climbing, and normal resting wing posture. (**b**) Bin3^{Y795A} is able to
995 bind and stabilize 7SK despite being catalytically-dead; consequently, Bin3^{Y795A} also promotes egg-
996 laying, climbing, and normal resting wing posture. (**c**) Bin3$^{\Delta MSM}$ binds, caps, and stabilizes 7SK, and

997 represses P-TEFb; this is sufficient to promote normal egg-laying and climbing, but is not sufficient to
998 promote normal wing posture. This suggests the MSM confers a 7SK-independent, tissue-specific
999 function to Bin3.
1000
1001 **Figure 8. Model for the role of Bin3 in *Drosophila* development.** **(a)** Bin3 binds, caps, and stabilizes
1002 7SK; however, methyltransferase activity is not required for 7SK stability *in vivo*. Stabilized 7SK
1003 assembles a snRNP that represses P-TEFb, which prevents RNAPII transcription elongation. **(b)** The
1004 Bin3 MSM confers a 7SK-independent, tissue-specific function to Bin3. The MSM might mediate an
1005 interaction with a tissue-specific factor, or this interaction might only be important in specific tissues.
1006 Bin3 and this factor then repress transcription elongation by a mechanism that is likely downstream of
1007 P-TEFb.

SUPPLEMENTAL TABLES

Table S1. Public fly stocks used in this study. This table lists the publicly available fly stocks used in this study, including their genotypes as they appear in the paper, their detailed genotypes, the stock center from which they were procured, and the stock number.

Table S2. Fly stocks produced for this study. This table lists the fly stocks produced for this study, including their genotypes as they appear in the paper, their detailed genotypes, and a detailed description of how each fly stock was produced.

Table S3. Flies used for experiments. This table lists the flies used in each figure, including their genotypes as they appear in the paper, their detailed genotypes, the genotypes of the female and male flies crossed to produce flies used for experiments, and the figure(s) in which each fly is used.

Table S4. DNA sequences. This table lists the names, sequences, and purposes of DNA primers and synthetic DNA constructs used for PCR, RT-PCR, RT-qPCR, and NEB Hi-Fi DNA Assembly.

1023 **REFERENCES**

1024 Abbaszadeh E. K., and E. R. Gavis, 2016 Fixed and live visualization of RNAs in Drosophila oocytes and
1025 embryos. Methods 98: 34–41. https://doi.org/10.1016/j.ymeth.2016.01.018

1026 Abuhashem A., V. Garg, and A.-K. Hadjantonakis, 2022 RNA polymerase II pausing in development:
1027 orchestrating transcription. Open Biol 12: 210220. https://doi.org/10.1098/rsob.210220

1028 Adelman K., and J. T. Lis, 2012 Promoter-proximal pausing of RNA polymerase II: emerging roles in
1029 metazoans. Nat Rev Genet 13: 720–731. https://doi.org/10.1038/nrg3293

1030 Akhtar J., Y. Renaud, S. Albrecht, Y. Ghavi-Helm, J.-Y. Roignant, *et al.*, 2021 m6A RNA methylation
1031 regulates promoter- proximal pausing of RNA polymerase II. Mol Cell 81: 3356-3367.e6.
1032 https://doi.org/10.1016/j.molcel.2021.06.023

1033 Ayala-Camargo A., A. M. Anderson, M. Amoyel, A. B. Rodrigues, M. S. Flaherty, *et al.*, 2013 JAK/STAT
1034 signaling is required for hinge growth and patterning in the Drosophila wing disc. Dev Biol 382: 413--
1035 426. https://doi.org/10.1016/j.ydbio.2013.08.016

1036 Baehrecke E. H., 1997 who encodes a KH RNA binding protein that functions in muscle development.
1037 Dev Camb Engl 124: 1323–32.

1038 Barboric M., T. Lenasi, H. Chen, E. B. Johansen, S. Guo, *et al.*, 2009 7SK snRNP/P-TEFb couples
1039 transcription elongation with alternative splicing and is essential for vertebrate development. Proc
1040 National Acad Sci 106: 7798–7803. https://doi.org/10.1073/pnas.0903188106

1041 Barrandon C., F. Bonnet, V. T. Nguyen, V. Labas, and O. Bensaude, 2007 The Transcription-Dependent
1042 Dissociation of P-TEFb-HEXIM1-7SK RNA Relies upon Formation of hnRNP-7SK RNA Complexes.
1043 Mol Cell Biol 27: 6996–7006. https://doi.org/10.1128/mcb.00975-07

1044 Blazek D., M. Barboric, J. Kohoutek, I. Oven, and B. M. Peterlin, 2005 Oligomerization of HEXIM1 via
1045 7SK snRNA and coiled-coil region directs the inhibition of P-TEFb. Nucleic Acids Res 33: 7000–7010.
1046 https://doi.org/10.1093/nar/gki997

1047 Brand A. H., and N. Perrimon, 1993 Targeted gene expression as a means of altering cell fates and
1048 generating dominant phenotypes. Development 118: 401–415.
1049 https://doi.org/10.1242/dev.118.2.401

1050 Brogie J. E., and D. H. Price, 2017 Reconstitution of a functional 7SK snRNP. Nucleic Acids Res 45: 6864–
1051 6880. https://doi.org/10.1093/nar/gkx262

1052 Brookes E., and A. Pombo, 2009 Modifications of RNA polymerase II are pivotal in regulating gene
1053 expression states. Embo Rep 10: 1213–1219. https://doi.org/10.1038/embor.2009.221

1054 Bugai A., A. J. C. Quaresma, C. C. Friedel, T. Lenasi, R. Düster, *et al.*, 2019 P-TEFb Activation by RBM7
1055 Shapes a Pro-survival Transcriptional Response to Genotoxic Stress. Mol Cell 74: 254-267.e10.
1056 https://doi.org/10.1016/j.molcel.2019.01.033

1057 Cabrera G. R., D. Godt, P. Fang, J. Couderc, and F. A. Laski, 2002 Expression pattern of Gal4 enhancer
1058 trap insertions into the bric à brac locus generated by P element replacement. Genesis 34: 62–65.
1059 https://doi.org/10.1002/gene.10115

Callus B. A., and B. Mathey-Prevot, 2002 SOCS36E, a novel Drosophila SOCS protein, suppresses JAK/STAT and EGF-R signalling in the imaginal wing disc. Oncogene 21: 4812--4821. https://doi.org/10.1038/sj.onc.1205618

Chan S.-K., and G. Struhl, 1997 Sequence-specific RNA binding by Bicoid. Nature 388: 634–634. https://doi.org/10.1038/41692

Chen F. X., E. R. Smith, and A. Shilatifard, 2018 Born to run: control of transcription elongation by RNA polymerase II. Nat Rev Mol Cell Bio 19: 464–478. https://doi.org/10.1038/s41580-018-0010-5

Cheng B., and D. H. Price, 2007 Properties of RNA Polymerase II Elongation Complexes Before and After the P-TEFb-mediated Transition into Productive Elongation*. J Biol Chem 282: 21901–21912. https://doi.org/10.1074/jbc.m702936200

Chiba K., J. Yamamoto, Y. Yamaguchi, and H. Handa, 2010 Promoter-proximal pausing and its release: Molecular mechanisms and physiological functions. Exp Cell Res 316: 2723–2730. https://doi.org/10.1016/j.yexcr.2010.05.036

Cho P. F., F. Poulin, Y. A. Cho-Park, I. B. Cho-Park, J. D. Chicoine, *et al.*, 2005 A New Paradigm for Translational Control: Inhibition via 5′-3′ mRNA Tethering by Bicoid and the eIF4E Cognate 4EHP. Cell 121: 411–423. https://doi.org/10.1016/j.cell.2005.02.024

Cook R. K., S. J. Christensen, J. A. Deal, R. A. Coburn, M. E. Deal, *et al.*, 2012 The generation of chromosomal deletions to provide extensive coverage and subdivision of the Drosophila melanogaster genome. Genome Biol 13: R21. https://doi.org/10.1186/gb-2012-13-3-r21

Core L., and K. Adelman, 2019 Promoter-proximal pausing of RNA polymerase II: a nexus of gene regulation. Gene Dev 33: 960–982. https://doi.org/10.1101/gad.325142.119

Cosgrove M. S., Y. Ding, W. A. Rennie, M. J. Lane, and S. D. Hanes, 2012 The Bin3 RNA methyltransferase targets 7SK RNA to control transcription and translation. Wiley Interdiscip Rev Rna 3: 633–647. https://doi.org/10.1002/wrna.1123

Deady L. D., and J. Sun, 2015 A Follicle Rupture Assay Reveals an Essential Role for Follicular Adrenergic Signaling in Drosophila Ovulation. Plos Genet 11: e1005604. https://doi.org/10.1371/journal.pgen.1005604

Diao F., and B. H. White, 2012 A Novel Approach for Directing Transgene Expression in Drosophila: T2A-Gal4 In-Frame Fusion. Genetics 190: 1139–1144. https://doi.org/10.1534/genetics.111.136291

Diao F., H. Ironfield, H. Luan, F. Diao, W. C. Shropshire, *et al.*, 2015 Plug-and-Play Genetic Access to Drosophila Cell Types using Exchangeable Exon Cassettes. Cell Reports 10: 1410–1421. https://doi.org/10.1016/j.celrep.2015.01.059

Dollinger R., and D. S. Gilmour, 2021 Regulation of Promoter Proximal Pausing of RNA Polymerase II in Metazoans. J Mol Biol 433: 166897. https://doi.org/10.1016/j.jmb.2021.166897

Doren M. V., A. L. Williamson, and R. Lehmann, 1998 Regulation of zygotic gene expression in Drosophila primordial germ cells. Curr Biol 8: 243–246. https://doi.org/10.1016/s0960-9822(98)70091-0

Dubnau J., and G. Struhl, 1996 RNA recognition and translational regulation by a homeodomain protein. Nature 379: 694–699. https://doi.org/10.1038/379694a0

Erdős G., and Z. Dosztányi, 2020 Analyzing Protein Disorder with IUPred2A. Curr Protoc Bioinform 70: e99. https://doi.org/10.1002/cpbi.99

Erdős G., M. Pajkos, and Z. Dosztányi, 2021 IUPred3: prediction of protein disorder enhanced with unambiguous experimental annotation and visualization of evolutionary conservation. Nucleic Acids Res 49: gkab408-. https://doi.org/10.1093/nar/gkab408

Fujinaga K., F. Huang, and B. M. Peterlin, 2023 P-TEFb: The master regulator of transcription elongation. Mol Cell 83: 393–403. https://doi.org/10.1016/j.molcel.2022.12.006

Gabler F., S. Nam, S. Till, M. Mirdita, M. Steinegger, *et al.*, 2020 Protein Sequence Analysis Using the MPI Bioinformatics Toolkit. Curr Protoc Bioinform 72: e108. https://doi.org/10.1002/cpbi.108

Gaertner B., and J. Zeitlinger, 2014 RNA polymerase II pausing during development. Development 141: 1179–1183. https://doi.org/10.1242/dev.088492

Garrett E. C., A. M. Bielawski, E. Ruchti, L. M. Sherer, I. Waghmare, *et al.*, 2023 The matricellular protein Drosophila CCN is required for synaptic transmission and female fertility. Genetics. https://doi.org/10.1093/genetics/iyac190

Gilmour D. S., 2009 Promoter proximal pausing on genes in metazoans. Chromosoma 118: 1–10. https://doi.org/10.1007/s00412-008-0182-4

Gonzalez M. N., D. Blears, and J. Q. Svejstrup, 2021 Causes and consequences of RNA polymerase II stalling during transcript elongation. Nat Rev Mol Cell Bio 22: 3–21. https://doi.org/10.1038/s41580-020-00308-8

Gupta S., R. K. Busch, R. Singh, and R. Reddy, 1990a Characterization of U6 small nuclear RNA cap-specific antibodies. Identification of gamma-monomethyl-GTP cap structure in 7SK and several other human small RNAs. J Biol Chem 265: 19137–19142. https://doi.org/10.1016/s0021-9258(17)30635-x

Gupta S., R. K. Busch, R. Singh, and R. Reddy, 1990b Characterization of U6 small nuclear RNA cap-specific antibodies. Identification of gamma-monomethyl-GTP cap structure in 7SK and several other human small RNAs. J Biological Chem 265: 19137–42.

Haaland R. E., C. H. Herrmann, and A. P. Rice, 2005 siRNA depletion of 7SK snRNA induces apoptosis but does not affect expression of the HIV-1 LTR or P-TEFb-dependent cellular genes. J Cell Physiol 205: 463–470. https://doi.org/10.1002/jcp.20528

Harrison D. A., P. E. McCoon, R. Binari, M. Gilman, and N. Perrimon, 1998 Drosophila unpaired encodes a secreted protein that activates the JAK signaling pathway. Gene Dev 12: 3252--3263. https://doi.org/10.1101/gad.12.20.3252

Hatini V., E. Kula-Eversole, D. Nusinow, and S. J. D. Signore, 2013 Essential roles for stat92E in expanding and patterning the proximodistal axis of the Drosophila wing imaginal disc. Dev Biol 378: 38--50. https://doi.org/10.1016/j.ydbio.2013.02.016

He N., N. S. Jahchan, E. Hong, Q. Li, M. A. Bayfield, *et al.*, 2008 A La-Related Protein Modulates 7SK snRNP Integrity to Suppress P-TEFb-Dependent Transcriptional Elongation and Tumorigenesis. Mol Cell 29: 588–599. https://doi.org/10.1016/j.molcel.2008.01.003

Herreweghe E. V., S. Egloff, I. Goiffon, B. E. Jády, C. Froment, *et al.*, 2007 Dynamic remodelling of human 7SK snRNP controls the nuclear level of active P-TEFb. Embo J 26: 3570–3580. https://doi.org/10.1038/sj.emboj.7601783

Hildebrand A., M. Remmert, A. Biegert, and J. Söding, 2009 Fast and accurate automatic structure prediction with HHpred. Proteins Struct Funct Bioinform 77: 128–132. https://doi.org/10.1002/prot.22499

Irizarry J., and A. Stathopoulos, 2015 FGF signaling supports Drosophila fertility by regulating development of ovarian muscle tissues. Dev Biol 404: 1–13. https://doi.org/10.1016/j.ydbio.2015.04.023

Jeronimo C., D. Forget, A. Bouchard, Q. Li, G. Chua, *et al.*, 2007 Systematic Analysis of the Protein Interaction Network for the Human Transcription Machinery Reveals the Identity of the 7SK Capping Enzyme. Mol Cell 27: 262–274. https://doi.org/10.1016/j.molcel.2007.06.027

Johnstone K., R. E. Wells, D. Strutt, and M. P. Zeidler, 2013 Localised JAK/STAT Pathway Activation Is Required for Drosophila Wing Hinge Development. Plos One 8. https://doi.org/10.1371/journal.pone.0065076

Jonkers I., and J. T. Lis, 2015 Getting up to speed with transcription elongation by RNA polymerase II. Nat Rev Mol Cell Bio 16: 167–177. https://doi.org/10.1038/nrm3953

Kairamkonda S., and U. Nongthomba, 2014 Beadex Function in the Motor Neurons Is Essential for Female Reproduction in Drosophila melanogaster. Plos One 9: e113003. https://doi.org/10.1371/journal.pone.0113003

Kan L., A. V. Grozhik, J. Vedanayagam, D. P. Patil, N. Pang, *et al.*, 2017 The m6A pathway facilitates sex determination in Drosophila. Nat Commun 8: 1--16. https://doi.org/10.1038/ncomms15737

Krueger B. J., C. Jeronimo, B. B. Roy, A. Bouchard, C. Barrandon, *et al.*, 2008 LARP7 is a stable component of the 7SK snRNP while P-TEFb, HEXIM1 and hnRNP A1 are reversibly associated. Nucleic Acids Res 36: 2219–2229. https://doi.org/10.1093/nar/gkn061

Krueger B. J., K. Varzavand, J. J. Cooper, and D. H. Price, 2010 The Mechanism of Release of P-TEFb and HEXIM1 from the 7SK snRNP by Viral and Cellular Activators Includes a Conformational Change in 7SK. Plos One 5: e12335. https://doi.org/10.1371/journal.pone.0012335

Lee P.-T., J. Zirin, O. Kanca, W.-W. Lin, K. L. Schulze, *et al.*, 2018 A gene-specific T2A-GAL4 library for Drosophila. Elife 7: e35574. https://doi.org/10.7554/elife.35574

Lee S., H. Liu, R. Hill, C. Chen, X. Hong, *et al.*, 2020 JMJD6 cleaves MePCE to release positive transcription elongation factor b (P-TEFb) in higher eukaryotes. Elife 9: e53930. https://doi.org/10.7554/elife.53930

Leger A., P. P. Amaral, L. Pandolfini, C. Capitanchik, F. Capraro, *et al.*, 2021 RNA modifications detection by comparative Nanopore direct RNA sequencing. Nat Commun 12: 7198. https://doi.org/10.1038/s41467-021-27393-3

Lemieux B., M. Blanchette, A. Monette, A. J. Mouland, R. J. Wellinger, *et al.*, 2015 A Function for the hnRNP A1/A2 Proteins in Transcription Elongation. Plos One 10: e0126654. https://doi.org/10.1371/journal.pone.0126654

Lence T., J. Akhtar, M. Bayer, K. Schmid, L. Spindler, *et al.*, 2016 m6A modulates neuronal functions and sex determination in Drosophila. Nature 540: 242–247. https://doi.org/10.1038/nature20568

Lence T., C. Paolantoni, L. Worpenberg, and J.-Y. Roignant, 2018 Mechanistic insights into m6A RNA enzymes. Biochimica Et Biophysica Acta Gene Regul Mech. https://doi.org/10.1016/j.bbagrm.2018.10.014

Levine M., 2011 Paused RNA Polymerase II as a Developmental Checkpoint. Cell 145: 502–511. https://doi.org/10.1016/j.cell.2011.04.021

Li Q., J. P. Price, S. A. Byers, D. Cheng, J. Peng, *et al.*, 2005 Analysis of the Large Inactive P-TEFb Complex Indicates That It Contains One 7SK Molecule, a Dimer of HEXIM1 or HEXIM2, and Two P-TEFb Molecules Containing Cdk9 Phosphorylated at Threonine 186*. J Biol Chem 280: 28819–28826. https://doi.org/10.1074/jbc.m502712200

Li J., and D. S. Gilmour, 2011 Promoter proximal pausing and the control of gene expression. Curr Opin Genet Dev 21: 231–235. https://doi.org/10.1016/j.gde.2011.01.010

Liao S., and D. R. Nässel, 2020 Drosophila Insulin-Like Peptide 8 (DILP8) in Ovarian Follicle Cells Regulates Ovulation and Metabolism. Front Endocrinol 11: 461. https://doi.org/10.3389/fendo.2020.00461

Liu X., W. L. Kraus, and X. Bai, 2015 Ready, pause, go: regulation of RNA polymerase II pausing and release by cellular signaling pathways. Trends Biochem Sci 40: 516–525. https://doi.org/10.1016/j.tibs.2015.07.003

Lobell A. S., R. R. Kaspari, Y. L. S. Negron, and S. T. Harbison, 2017 The Genetic Architecture of Ovariole Number in Drosophila melanogaster: Genes with Major, Quantitative, and Pleiotropic Effects. G3 Genes Genomes Genetics 7: 2391–2403. https://doi.org/10.1534/g3.117.042390

Maimon I., and L. Gilboa, 2011 Dissection and Staining of Drosophila Larval Ovaries. J Vis Exp. https://doi.org/10.3791/2537

Manjila S., and G. Hasan, 2018 Flight and Climbing Assay for Assessing Motor Functions in Drosophila. Bio-protocol 8. https://doi.org/10.21769/bioprotoc.2742

Margaritis T., and F. C. P. Holstege, 2008 Poised RNA Polymerase II Gives Pause for Thought. Cell 133: 581–584. https://doi.org/10.1016/j.cell.2008.04.027

Markert A., M. Grimm, J. Martinez, J. Wiesner, A. Meyerhans, *et al.*, 2008 The La-related protein LARP7 is a component of the 7SK ribonucleoprotein and affects transcription of cellular and viral polymerase II genes. Embo Rep 9: 569–575. https://doi.org/10.1038/embor.2008.72

Marshall N. F., and D. H. Price, 1995 Purification of P-TEFb, a Transcription Factor Required for the Transition into Productive Elongation (∗). J Biol Chem 270: 12335–12338. https://doi.org/10.1074/jbc.270.21.12335

Marshall N. F., J. Peng, Z. Xie, and D. H. Price, 1996 Control of RNA Polymerase II Elongation Potential by a Novel Carboxyl-terminal Domain Kinase*. J Biol Chem 271: 27176–27183. https://doi.org/10.1074/jbc.271.43.27176

1213 Mayer A., H. M. Landry, and L. S. Churchman, 2017 Pause & go: from the discovery of RNA polymerase
1214 pausing to its functional implications. Curr Opin Cell Biol 46: 72–80.
1215 https://doi.org/10.1016/j.ceb.2017.03.002

1216 Meier A., and J. Söding, 2015 Automatic Prediction of Protein 3D Structures by Probabilistic Multi-
1217 template Homology Modeling. Plos Comput Biol 11: e1004343.
1218 https://doi.org/10.1371/journal.pcbi.1004343

1219 Mészáros B., G. Erdős, and Z. Dosztányi, 2018 IUPred2A: context-dependent prediction of protein
1220 disorder as a function of redox state and protein binding. Nucleic Acids Res 46: gky384-.
1221 https://doi.org/10.1093/nar/gky384

1222 Michels A. A., A. Fraldi, Q. Li, T. E. Adamson, F. Bonnet, *et al.*, 2004 Binding of the 7SK snRNA turns the
1223 HEXIM1 protein into a P-TEFb (CDK9/cyclin T) inhibitor. Embo J 23: 2608–2619.
1224 https://doi.org/10.1038/sj.emboj.7600275

1225 Muniz L., S. Egloff, and T. Kiss, 2013 RNA elements directing in vivo assembly of the 7SK/MePCE/Larp7
1226 transcriptional regulatory snRNP. Nucleic Acids Res 41: 4686–4698.
1227 https://doi.org/10.1093/nar/gkt159

1228 Murphy S., M. Tripodi, and M. Melli, 1986 A sequence upstream from the coding region is required for
1229 the transcription of the 7SK RNA genes. Nucleic Acids Res 14: 9243–9260.
1230 https://doi.org/10.1093/nar/14.23.9243

1231 Murphy S., C. D. Liegro, and M. Melli, 1987 The in vitro transcription of the 7SK RNA gene by RNA
1232 polymerase III is dependent only on the presence of an upstream promoter. Cell 51: 81–87.
1233 https://doi.org/10.1016/0092-8674(87)90012-2

Murphy S., A. Pierani, C. Scheidereit, M. Melli, and R. G. Roeder, 1989 Purified octamer binding transcription factors stimulate RNA polymerase III-mediated transcription of the 7SK RNA gene. Cell 59: 1071–1080. https://doi.org/10.1016/0092-8674(89)90763-0

Nechaev S., and K. Adelman, 2011 Pol II waiting in the starting gates: Regulating the transition from transcription initiation into productive elongation. Biochimica Et Biophysica Acta Bba - Gene Regul Mech 1809: 34–45. https://doi.org/10.1016/j.bbagrm.2010.11.001

Nguyen V. T., T. Kiss, A. A. Michels, and O. Bensaude, 2001 7SK small nuclear RNA binds to and inhibits the activity of CDK9/cyclin T complexes. Nature 414: 322–325. https://doi.org/10.1038/35104581

Nguyen D., B. J. Krueger, S. C. Sedore, J. E. Brogie, J. T. Rogers, *et al.*, 2012 The Drosophila 7SK snRNP and the essential role of dHEXIM in development. Nucleic Acids Res 40: 5283–5297. https://doi.org/10.1093/nar/gks191

Ni Z., B. E. Schwartz, J. Werner, J.-R. Suarez, and J. T. Lis, 2004 Coordination of Transcription, RNA Processing, and Surveillance by P-TEFb Kinase on Heat Shock Genes. Mol Cell 13: 55–65. https://doi.org/10.1016/s1097-2765(03)00526-4

Ni Z., A. Saunders, N. J. Fuda, J. Yao, J.-R. Suarez, *et al.*, 2008 P-TEFb Is Critical for the Maturation of RNA Polymerase II into Productive Elongation In Vivo. Mol Cell Biol 28: 1161–1170. https://doi.org/10.1128/mcb.01859-07

Ni J. Q., R. Zhou, B. Czech, L. P. Liu, L. Holderbaum, *et al.*, 2011 A genome-scale shRNA resource for transgenic RNAi in Drosophila. Nat Methods 8: 405--407. https://doi.org/10.1038/nmeth.1592

Niessing D., N. Dostatni, H. Jäckle, and R. Rivera-Pomar, 1999 Sequence interval within the PEST motif of Bicoid is important for translational repression of caudal mRNA in the anterior region of the Drosophila embryo. Embo J 18: 1966–1973. https://doi.org/10.1093/emboj/18.7.1966

Niessing D., W. Driever, F. Sprenger, H. Taubert, H. Jäckle, *et al.*, 2000 Homeodomain Position 54 Specifies Transcriptional versus Translational Control by Bicoid. Mol Cell 5: 395–401. https://doi.org/10.1016/s1097-2765(00)80434-7

Niessing D., S. Blanke, and H. Jäckle, 2002 Bicoid associates with the 5′-cap-bound complex of caudal mRNA and represses translation. Gene Dev 16: 2576–2582. https://doi.org/10.1101/gad.240002

Páez-Moscoso D. J., D. V. Ho, L. Pan, K. Hildebrand, K. L. Jensen, *et al.*, 2022 A putative cap binding protein and the methyl phosphate capping enzyme Bin3/MePCE function in telomerase biogenesis. Nat Commun 13: 1067. https://doi.org/10.1038/s41467-022-28545-9

Parks A. L., K. R. Cook, M. Belvin, N. A. Dompe, R. Fawcett, *et al.*, 2004 Systematic generation of high-resolution deletion coverage of the Drosophila melanogaster genome. Nat Genet 36: 288--292. https://doi.org/10.1038/ng1312

Peng J., N. F. Marshall, and D. H. Price, 1998 Identification of a Cyclin Subunit Required for the Function ofDrosophila P-TEFb*. J Biol Chem 273: 13855–13860. https://doi.org/10.1074/jbc.273.22.13855

Perez-Pepe M., A. W. Desotell, H. Li, W. Li, B. Han, *et al.*, 2023 7SK methylation by METTL3 promotes transcriptional activity. Sci Adv 9. https://doi.org/10.1126/sciadv.ade7500

Peterlin B. M., J. E. Brogie, and D. H. Price, 2011 7SK snRNA: a noncoding RNA that plays a major role in regulating eukaryotic transcription. Wiley Interdiscip Rev Rna 3: 92–103. https://doi.org/10.1002/wrna.106

Pfeiffer B. D., A. Jenett, A. S. Hammonds, T.-T. B. Ngo, S. Misra, *et al.*, 2008 Tools for neuroanatomy and neurogenetics in Drosophila. Proc National Acad Sci 105: 9715–9720. https://doi.org/10.1073/pnas.0803697105

Porat J., M. E. Baidouri, J. Grigull, J.-M. Deragon, and M. A. Bayfield, 2022 The methyl phosphate capping enzyme Bmc1/Bin3 is a stable component of the fission yeast telomerase holoenzyme. Nat Commun 13: 1277. https://doi.org/10.1038/s41467-022-28985-3

Qiao H. H., F. Wang, R. G. Xu, J. Sun, R. Zhu, *et al.*, 2018 An efficient and multiple target transgenic RNAi technique with low toxicity in Drosophila. Nat Commun 9. https://doi.org/10.1038/s41467-018-06537-y

Raj A., and S. Tyagi, 2010 Single Molecule Tools: Fluorescence Based Approaches, Part A. Methods Enzymol 472: 365–386. https://doi.org/10.1016/s0076-6879(10)72004-8

Ramanathan Y., S. M. Rajpara, S. M. Reza, E. Lees, S. Shuman, *et al.*, 2001 Three RNA Polymerase II Carboxyl-terminal Domain Kinases Display Distinct Substrate Preferences*. J Biol Chem 276: 10913–10920. https://doi.org/10.1074/jbc.m010975200

Rivera-Pomar R., D. Niessing, U. Schmidt-Ott, W. J. Gehring, and H. Jäckle, 1996 RNA binding and translational suppression by bicoid. Nature 379: 746–9. https://doi.org/10.1038/379746a0

Ryder E., F. Blows, M. Ashburner, R. Bautista-Llacer, D. Coulson, *et al.*, 2004 The DrosDel collection: A set of P-element insertions for generating custom chromosomal aberrations in Drosophila melanogaster. Genetics 167: 797--813. https://doi.org/10.1534/genetics.104.026658

Sahut-Barnola I., D. Godt, F. A. Laski, and J.-L. Couderc, 1995 Drosophila Ovary Morphogenesis: Analysis of Terminal Filament Formation and Identification of a Gene Required for This Process. Dev Biol 170: 127–135. https://doi.org/10.1006/dbio.1995.1201

Sahut-Barnola I., B. Dastugue, and J.-L. Couderc, 1996 Terminal filament cell organization in the larval ovary of Drosophila melanogaster: ultrastructural observations and pattern of divisions. Roux's Archives Dev Biology 205: 356–363. https://doi.org/10.1007/bf00377215

Šali A., L. Potterton, F. Yuan, H. van Vlijmen, and M. Karplus, 1995 Evaluation of comparative protein modeling by MODELLER. Proteins Struct Funct Bioinform 23: 318–326. https://doi.org/10.1002/prot.340230306

Sanhueza M., L. Zechini, T. Gillespie, and G. Pennetta, 2014 Gain-of-function mutations in the ALS8 causative gene VAPB have detrimental effects on neurons and muscles. Biol Open 3: 59--71. https://doi.org/10.1242/bio.20137070

Schneeberger P. E., T. Bierhals, A. Neu, M. Hempel, and K. Kutsche, 2019 de novo MEPCE nonsense variant associated with a neurodevelopmental disorder causes disintegration of 7SK snRNP and enhanced RNA polymerase II activation. Sci Rep-uk 9: 12516. https://doi.org/10.1038/s41598-019-49032-0

Shelton S. B., N. M. Shah, N. S. Abell, S. K. Devanathan, M. Mercado, *et al.*, 2018 Crosstalk between the RNA Methylation and Histone-Binding Activities of MePCE Regulates P-TEFb Activation on Chromatin. Cell Reports 22: 1374–1383. https://doi.org/10.1016/j.celrep.2018.01.028

Shim E. Y., A. K. Walker, Y. Shi, and T. K. Blackwell, 2002 CDK-9/cyclin T (P-TEFb) is required in two postinitiation pathways for transcription in the C. elegans embryo. Gene Dev 16: 2135–2146. https://doi.org/10.1101/gad.999002

Shimba S., and R. Reddy, 1994 Purification of human U6 small nuclear RNA capping enzyme. Evidence for a common capping enzyme for gamma-monomethyl-capped small RNAs. J Biological Chem 269: 12419–23.

Shukla V., F. Habib, A. Kulkarni, and G. S. Ratnaparkhi, 2013 Gene Duplication, Lineage-Specific Expansion, and Subfunctionalization in the MADF-BESS Family Patterns the Drosophila Wing Hinge. Genetics 196: 481–496. https://doi.org/10.1534/genetics.113.160531

Shumyatsky G. P., S. V. Tillib, and D. A. Kramerov, 1990 B2 RNA and 7SK RNA, RNA polymerase III transcripts, have a cap-like structure at their 5′ end. Nucleic Acids Res 18: 6347–6351. https://doi.org/10.1093/nar/18.21.6347

Shumyatsky G., D. Wright, and R. Reddy, 1993 Methylphosphate cap structure increases the stability of 7SK, B2 and U6 small RNAs in Xenopus oocytes. Nucleic Acids Res 21: 4756–4761. https://doi.org/10.1093/nar/21.20.4756

Shumyatsky G., S. Shimba, and R. Reddy, 1994 Capping signals correspond to the 5′ end in four eukaryotic small RNAs containing gamma-monomethylphosphate cap structure. Gene Expression 4: 29--41.

Singh R., S. Gupta, and R. Reddy, 1990 Capping of Mammalian U6 Small Nuclear RNA In Vitro Is Directed by a Conserved Stem-Loop and AUAUAC Sequence: Conversion of a Noncapped RNA into a Capped RNA. Mol Cell Biol 10: 939–946. https://doi.org/10.1128/mcb.10.3.939-946.1990

Singh N., H. Morlock, and S. D. Hanes, 2011 The Bin3 RNA methyltransferase is required for repression of caudal translation in the Drosophila embryo. Dev Biol 352: 104–115. https://doi.org/10.1016/j.ydbio.2011.01.017

Söding J., 2005 Protein homology detection by HMM–HMM comparison. Bioinformatics 21: 951–960. https://doi.org/10.1093/bioinformatics/bti125

Spradling A. C., D. Stern, A. Beaton, E. J. Rhem, T. Laverty, *et al.*, 1999 The Berkeley Drosophila Genome Project Gene Disruption Project: Single P-Element Insertions Mutating 25% of Vital Drosophila Genes. Genetics 153: 135–177. https://doi.org/10.1093/genetics/153.1.135

Takeo S., S. K. Swanson, K. Nandanan, Y. Nakai, T. Aigaki, *et al.*, 2012 Shaggy/glycogen synthase kinase 3β and phosphorylation of Sarah/regulator of calcineurin are essential for completion of Drosophila female meiosis. Proc National Acad Sci 109: 6382–6389. https://doi.org/10.1073/pnas.1120367109

Wada T., T. Takagi, Y. Yamaguchi, D. Watanabe, and H. Handa, 1998 Evidence that P-TEFb alleviates the negative effect of DSIF on RNA polymerase II-dependent transcription in vitro. Embo J 17: 7395–7403. https://doi.org/10.1093/emboj/17.24.7395

Wang X., S. Hang, L. Prazak, and J. P. Gergen, 2010 NELF Potentiates Gene Transcription in the Drosophila Embryo. Plos One 5: e11498. https://doi.org/10.1371/journal.pone.0011498

Wang S., P. Chai, R. Jia, and R. Jia, 2018 Novel insights on m6A RNA methylation in tumorigenesis: a double-edged sword. Mol Cancer 17: 101. https://doi.org/10.1186/s12943-018-0847-4

Wang F., H.-H. Qiao, R.-G. Xu, J. Sun, R. Zhu, *et al.*, 2019 pNP Transgenic RNAi System Manual in Drosophila. Bio-protocol 9: 1--12. https://doi.org/10.21769/bioprotoc.3158

Warda A. S., J. Kretschmer, P. Hackert, C. Lenz, H. Urlaub, *et al.*, 2017 Human METTL16 is a N6-methyladenosine (m6A) methyltransferase that targets pre-mRNAs and various non-coding RNAs. Embo Rep 18: 2004–2014. https://doi.org/10.15252/embr.201744940

Wayne M. L., J. B. Hackett, and T. F. C. Mackay, 1997 QUANTITATIVE GENETICS OF OVARIOLE NUMBER IN DROSOPHILA MELANOGASTER. I. SEGREGATING VARIATION AND FITNESS. Evolution 51: 1156–1163. https://doi.org/10.1111/j.1558-5646.1997.tb03963.x

Wayne M. L., and T. F. C. Mackay, 1998 Quantitative Genetics of Ovariole Number in Drosophila melanogaster. II. Mutational Variation and Genotype-Environment Interaction. Genetics 148: 201–210. https://doi.org/10.1093/genetics/148.1.201

Xu X., L. Ma, X. Zhang, S. Guo, W. Guo, *et al.*, 2022 A positive feedback circuit between RN7SK snRNA and m6A readers is essential for tumorigenesis. Mol Ther J Am Soc Gene Ther. https://doi.org/10.1016/j.ymthe.2022.12.013

Xue Y., Z. Yang, R. Chen, and Q. Zhou, 2010 A capping-independent function of MePCE in stabilizing 7SK snRNA and facilitating the assembly of 7SK snRNP. Nucleic Acids Res 38: 360–369. https://doi.org/10.1093/nar/gkp977

Yamaguchi Y., T. Takagi, T. Wada, K. Yano, A. Furuya, *et al.*, 1999 NELF, a Multisubunit Complex Containing RD, Cooperates with DSIF to Repress RNA Polymerase II Elongation. Cell 97: 41–51. https://doi.org/10.1016/s0092-8674(00)80713-8

Yang Z., Q. Zhu, K. Luo, and Q. Zhou, 2001 The 7SK small nuclear RNA inhibits the CDK9/cyclin T1 kinase to control transcription. Nature 414: 317–322. https://doi.org/10.1038/35104575

Yang Y., C. D. Eichhorn, Y. Wang, D. Cascio, and J. Feigon, 2019 Structural basis of 7SK RNA 5′-γ-phosphate methylation and retention by MePCE. Nat Chem Biol 15: 132–140. https://doi.org/10.1038/s41589-018-0188-z

Yang Y., S. Liu, S. Egloff, C. D. Eichhorn, T. Hadjian, *et al.*, 2022 Structural basis of RNA conformational switching in the transcriptional regulator 7SK RNP. Mol Cell 82: 1724-1736.e7. https://doi.org/10.1016/j.molcel.2022.03.001

Yik J. H. N., R. Chen, A. C. Pezda, C. S. Samford, and Q. Zhou, 2004 A Human Immunodeficiency Virus Type 1 Tat-Like Arginine-Rich RNA-Binding Domain Is Essential for HEXIM1 To Inhibit RNA Polymerase II Transcription through 7SK snRNA-Mediated Inactivation of P-TEFb. Mol Cell Biol 24: 5094–5105. https://doi.org/10.1128/mcb.24.12.5094-5105.2004

Zhang B., Z. Liu, J. Liu, K. Cao, W. Shan, *et al.*, 2021 Long non-coding RNA ST8SIA6-AS1 promotes the migration and invasion of hypoxia-treated hepatocellular carcinoma cells through the miR-338/MEPCE axis. Oncol Rep 45: 73–82. https://doi.org/10.3892/or.2020.7864

Zhou M., M. A. Halanski, M. F. Radonovich, F. Kashanchi, J. Peng, *et al.*, 2000 Tat Modifies the Activity of CDK9 To Phosphorylate Serine 5 of the RNA Polymerase II Carboxyl-Terminal Domain during

Human Immunodeficiency Virus Type 1 Transcription. Mol Cell Biol 20: 5077–5086. https://doi.org/10.1128/mcb.20.14.5077-5086.2000

Zhou Q., T. Li, and D. H. Price, 2012 RNA Polymerase II Elongation Control. Biochemistry-us 81: 119–143. https://doi.org/10.1146/annurev-biochem-052610-095910

Zhu W., and S. D. Hanes, 2000 Identification of Drosophila Bicoid-interacting proteins using a custom two-hybrid selection. Gene 245: 329–339. https://doi.org/10.1016/s0378-1119(00)00048-2

Zieve G., and S. Penman, 1976 Small RNA species of the HeLa cell: Metabolism and subcellular localization. Cell 8: 19–31. https://doi.org/10.1016/0092-8674(76)90181-1

Zimmermann L., A. Stephens, S.-Z. Nam, D. Rau, J. Kübler, *et al.*, 2018 A Completely Reimplemented MPI Bioinformatics Toolkit with a New HHpred Server at its Core. J Mol Biol 430: 2237–2243. https://doi.org/10.1016/j.jmb.2017.12.007

Fig. 1

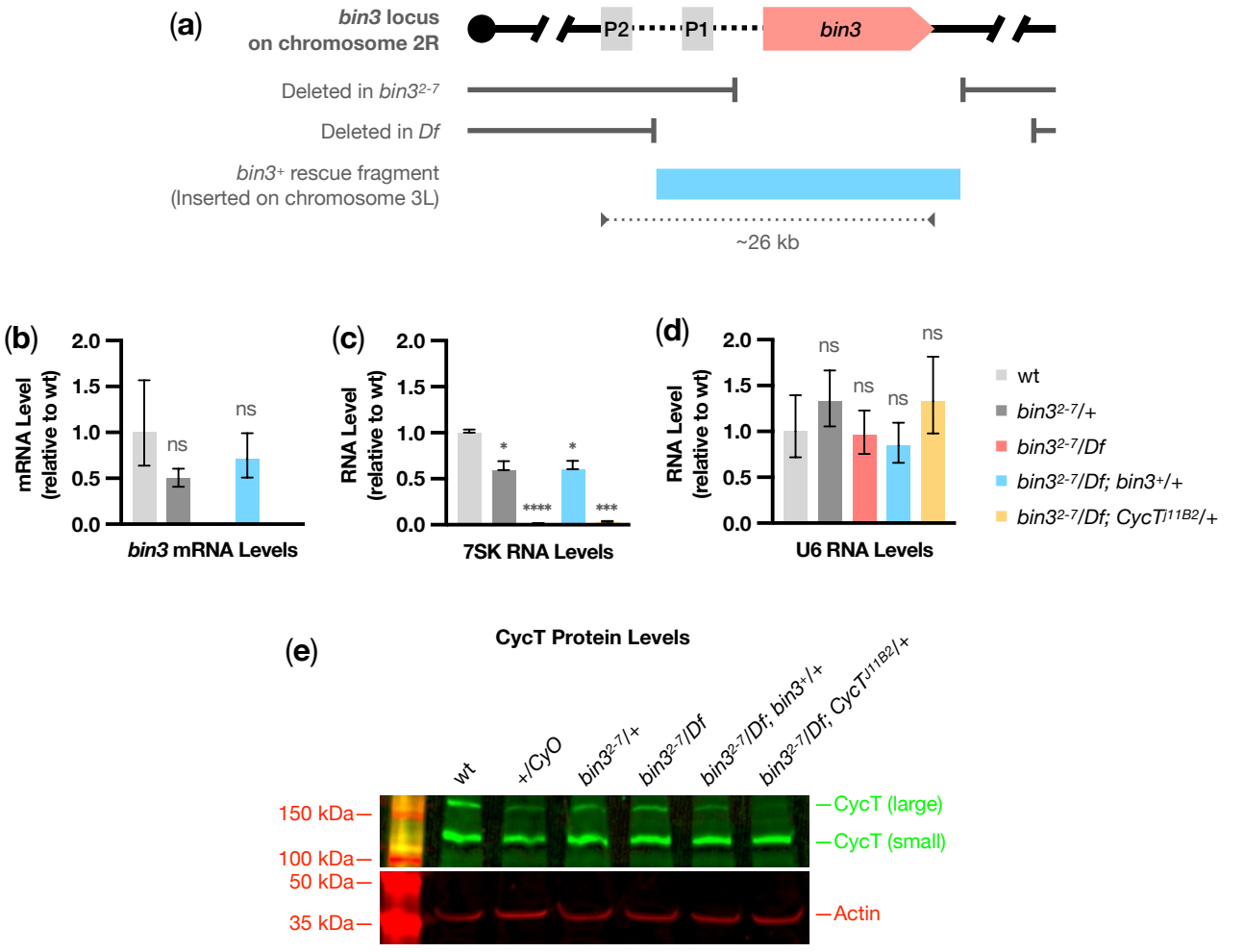
(a)
bin3 locus on chromosome 2R
P2
P1
bin3
Deleted in bin3 2-7
Deleted in Df
bin3+ rescue fragment (Inserted on chromosome 3L)
~26 kb
(b)
mRNA Level (relative to wt)
2.0
1.5
1.0
0.5
0.0
ns
ns
bin3 mRNA Levels
(c)
RNA Level (relative to wt)
*
****
*
***
7SK RNA Levels
(d)
RNA Level (relative to wt)
ns
ns
ns
ns
U6 RNA Levels
wt
bin3 2-7/+
bin3 2-7/Df
bin3 2-7/Df; bin3+/+
bin3 2-7/Df; CycT J11B2/+
(e)
CycT Protein Levels
wt
+/CyO
bin3 2-7/+
bin3 2-7/Df
bin3 2-7/Df; bin3+/+
bin3 2-7/Df; CycT J11B2/+
150 kDa
100 kDa
50 kDa
35 kDa
CycT (large)
CycT (small)
Actin

Fig. 2

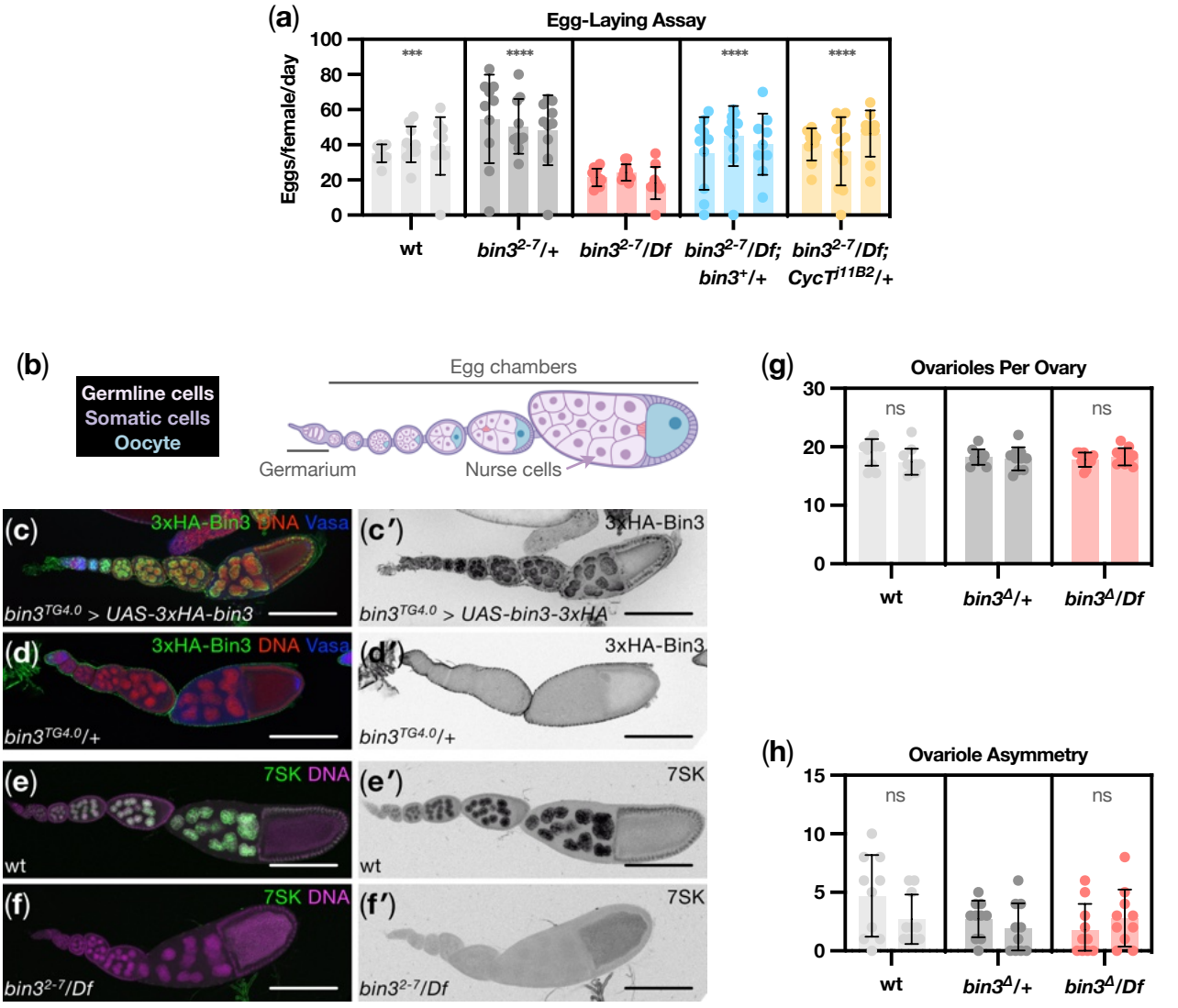
(a)
Egg-Laying Assay
Eggs/female/day
100
80
60
40
20
0
***
****
****
****
wt
bin3^2-7/+
bin3^2-7/Df
bin3^2-7/Df; bin3^+/+
bin3^2-7/Df; CycT^j11B2/+
(b)
Germline cells
Somatic cells
Oocyte
Egg chambers
Germarium
Nurse cells
(c)
3xHA-Bin3 DNA Vasa
bin3^TG4.0 > UAS-3xHA-bin3
(c′)
3xHA-Bin3
bin3^TG4.0 > UAS-bin3-3xHA
(d)
3xHA-Bin3 DNA Vasa
bin3^TG4.0/+
(d′)
3xHA-Bin3
bin3^TG4.0/+
(e)
7SK DNA
wt
(e′)
7SK
wt
(f)
7SK DNA
bin3^2-7/Df
(f′)
7SK
bin3^2-7/Df
(g)
Ovarioles Per Ovary
30
20
10
0
ns
ns
wt
bin3^Δ/+
bin3^Δ/Df
(h)
Ovariole Asymmetry
15
10
5
0
ns
ns
wt
bin3^Δ/+
bin3^Δ/Df
(i)
Egg-laying Assay with
Germline-Specific Bin3 expression
Eggs/female/day
120
100
80
60
40
20
0
*
***
ns
wt
bin3^2-7/+; nos-GAL4::VP16/+
bin3^2-7/Df; nos-GAL4::VP16/+
bin3^2-7/Df; nos-GAL4::VP16/UAS-bin3

Fig. 3

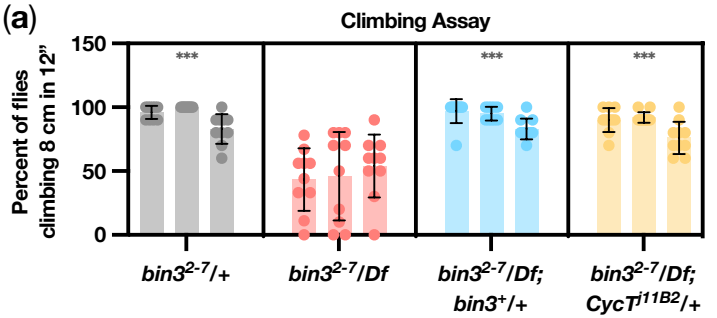
(a)
Climbing Assay
Percent of flies climbing 8 cm in 12"
150
100
50
0
***
***
***
bin3²⁻⁷/+
bin3²⁻⁷/Df
bin3²⁻⁷/Df; bin3⁺/+
bin3²⁻⁷/Df; CycT^j11B2/+

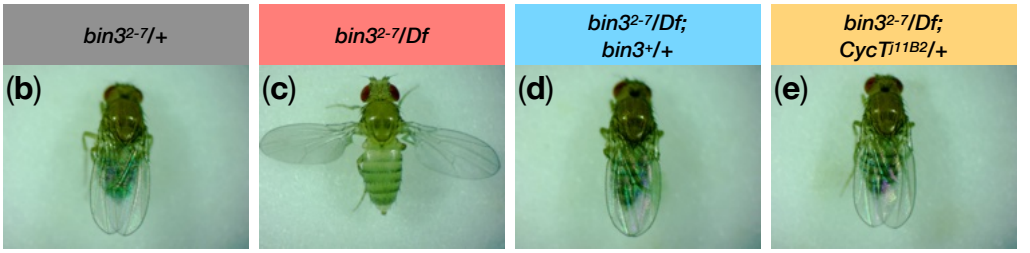
bin3²⁻⁷/+
(b)
bin3²⁻⁷/Df
(c)
bin3²⁻⁷/Df; bin3⁺/+
(d)
bin3²⁻⁷/Df; CycT^j11B2/+
(e)

Fig. 4

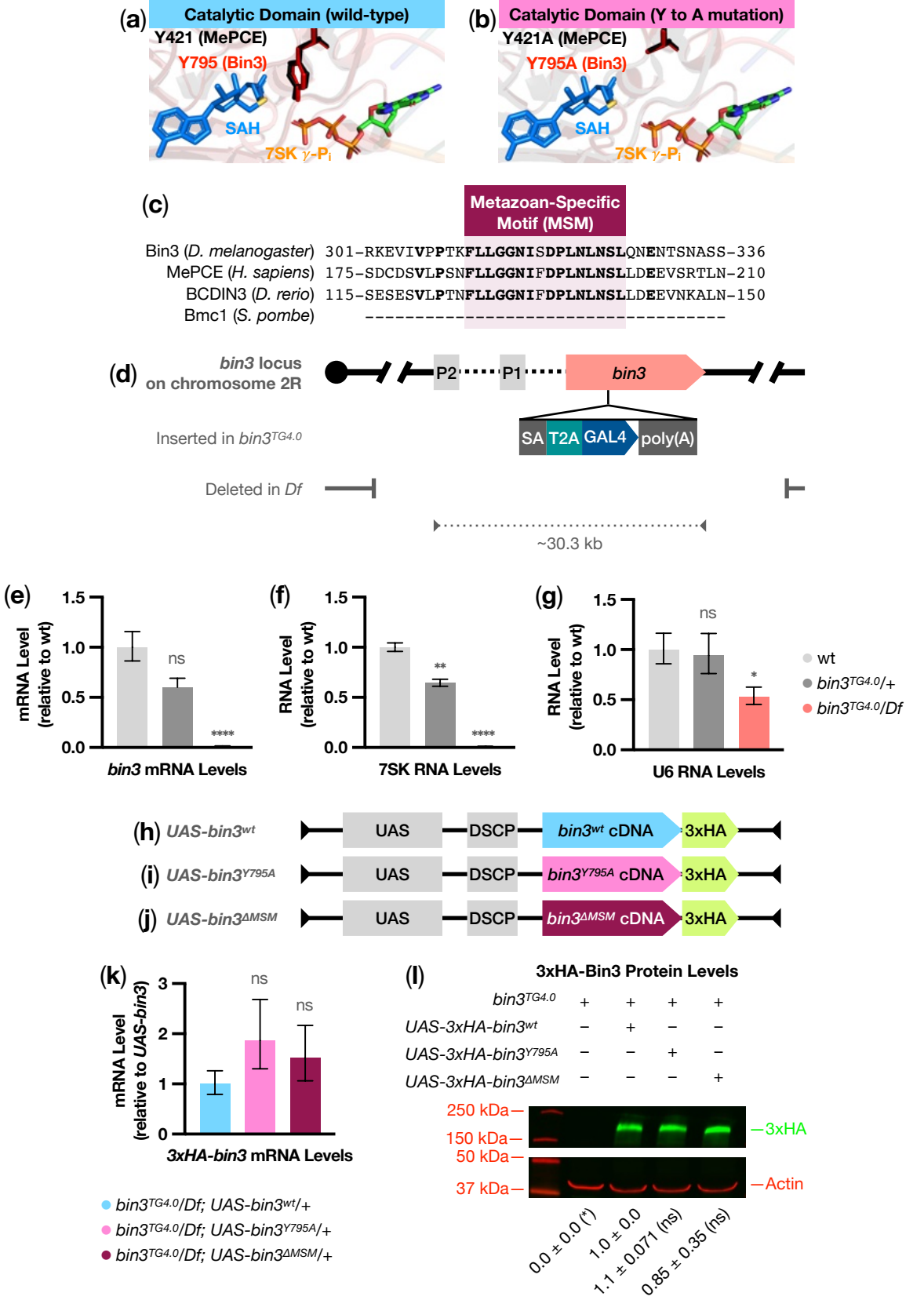
(a)
Catalytic Domain (wild-type)
Y421 (MePCE)
Y795 (Bin3)
SAH
7SK γ-Pi
(b)
Catalytic Domain (Y to A mutation)
Y421A (MePCE)
Y795A (Bin3)
SAH
7SK γ-Pi
(c)
Metazoan-Specific Motif (MSM)
Bin3 (D. melanogaster) 301-RKEVIVPPTKFLLGGNISDPLNLNSLQNENTSNASS-336
MePCE (H. sapiens) 175-SDCDSVLPSNFLLGGNIFDPLNLNSLLDEEVSRTLN-210
BCDIN3 (D. rerio) 115-SESESVLPTNFLLGGNIFDPLNLNSLLDEEVNKALN-150
Bmc1 (S. pombe) ----------
(d)
bin3 locus on chromosome 2R
P2
P1
bin3
Inserted in bin3TG4.0
SA
T2A
GAL4
poly(A)
Deleted in Df
~30.3 kb
(e)
mRNA Level (relative to wt)
1.5
1.0
0.5
0.0
ns
****
bin3 mRNA Levels
(f)
RNA Level (relative to wt)
**
****
7SK RNA Levels
(g)
ns
*
U6 RNA Levels
wt
bin3TG4.0/+
bin3TG4.0/Df
(h) UAS-bin3wt
(i) UAS-bin3Y795A
(j) UAS-bin3ΔMSM
UAS
DSCP
bin3wt cDNA
bin3Y795A cDNA
bin3ΔMSM cDNA
3xHA
(k)
mRNA Level (relative to UAS-bin3)
3
2
1
0
ns
ns
3xHA-bin3 mRNA Levels
bin3TG4.0/Df; UAS-bin3wt/+
bin3TG4.0/Df; UAS-bin3Y795A/+
bin3TG4.0/Df; UAS-bin3ΔMSM/+
(l)
3xHA-Bin3 Protein Levels
bin3TG4.0 + + + +
UAS-3xHA-bin3wt − + − −
UAS-3xHA-bin3Y795A − − + −
UAS-3xHA-bin3ΔMSM − − − +
250 kDa
150 kDa
50 kDa
37 kDa
3xHA
Actin
0.0 ± 0.0 (*)
1.0 ± 0.0
1.1 ± 0.071 (ns)
0.85 ± 0.35 (ns)

Fig. 5

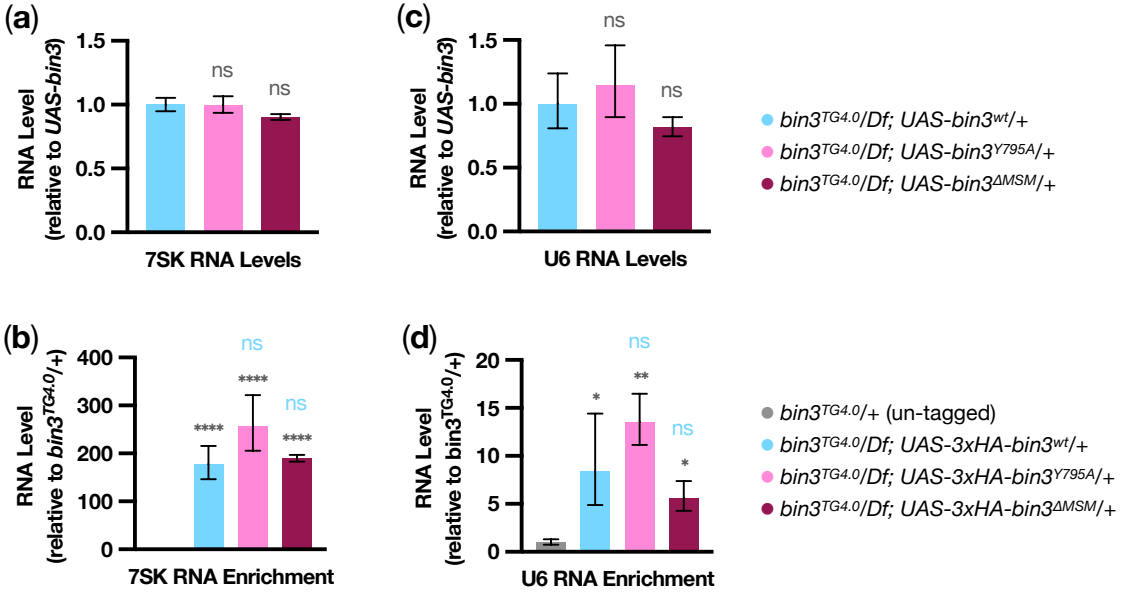
(a)
RNA Level
(relative to UAS-bin3)
1.5
1.0
0.5
0.0
ns
ns
7SK RNA Levels
(c)
RNA Level
(relative to UAS-bin3)
1.5
1.0
0.5
0.0
ns
ns
U6 RNA Levels
bin3TG4.0/Df; UAS-bin3wt/+
bin3TG4.0/Df; UAS-bin3Y795A/+
bin3TG4.0/Df; UAS-bin3ΔMSM/+
(b)
RNA Level
(relative to bin3TG4.0/+)
400
300
200
100
0
ns
****
****
ns
****
7SK RNA Enrichment
(d)
RNA Level
(relative to bin3TG4.0/+)
20
15
10
5
0
ns
*
**
ns
*
U6 RNA Enrichment
bin3TG4.0/+ (un-tagged)
bin3TG4.0/Df; UAS-3xHA-bin3wt/+
bin3TG4.0/Df; UAS-3xHA-bin3Y795A/+
bin3TG4.0/Df; UAS-3xHA-bin3ΔMSM/+

Fig. 6

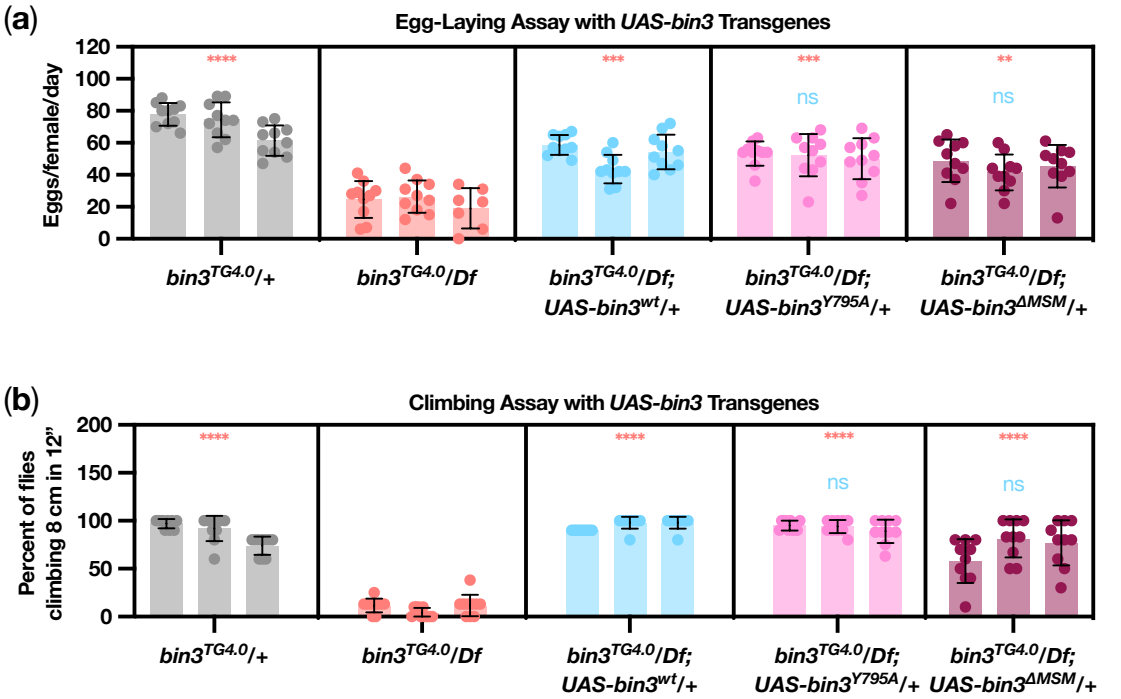
(a)
Egg-Laying Assay with UAS-bin3 Transgenes
Eggs/female/day
120
100
80
60
40
20
0
****
***
***
ns
**
ns
bin3TG4.0/+
bin3TG4.0/Df
bin3TG4.0/Df; UAS-bin3wt/+
bin3TG4.0/Df; UAS-bin3Y795A/+
bin3TG4.0/Df; UAS-bin3ΔMSM/+
(b)
Climbing Assay with UAS-bin3 Transgenes
Percent of flies climbing 8 cm in 12"
200
150
100
50
0
****
****
****
ns
****
ns
bin3TG4.0/+
bin3TG4.0/Df
bin3TG4.0/Df; UAS-bin3wt/+
bin3TG4.0/Df; UAS-bin3Y795A/+
bin3TG4.0/Df; UAS-bin3ΔMSM/+

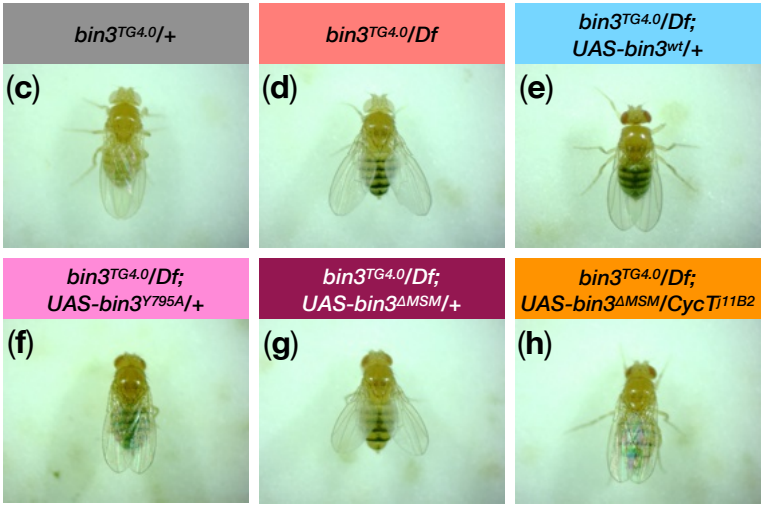
bin3TG4.0/+
(c)
bin3TG4.0/Df
(d)
bin3TG4.0/Df; UAS-bin3wt/+
(e)
bin3TG4.0/Df; UAS-bin3Y795A/+
(f)
bin3TG4.0/Df; UAS-bin3ΔMSM/+
(g)
bin3TG4.0/Df; UAS-bin3ΔMSM/CycTj11B2
(h)

Fig. 7

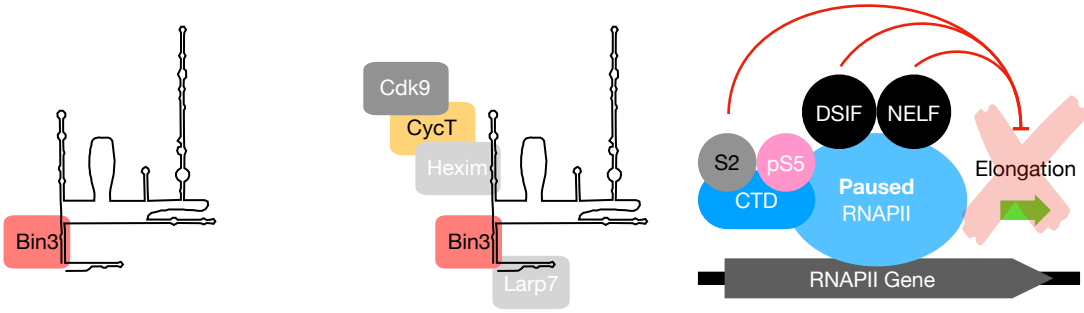

		Bin3 binds 7SK	Bin3 caps 7SK	Bin3 stabilizes 7SK	7SK snRNP assembles and represses P-TEFb	Repressed P-TEFb promotes RNAPII pausing to support…		
						Fecundity	Climbing	Wing posture
(a)	Bin3^{wt}	✓	✓	✓	✓	✓	✓	✓
(b)	Bin3^{Y795A}	✓	✗	✓	✓	✓	✓	✓
(c)	Bin3^{MSM}	✓	✓	✓	✓	✓	✓	✗

Fig. 8

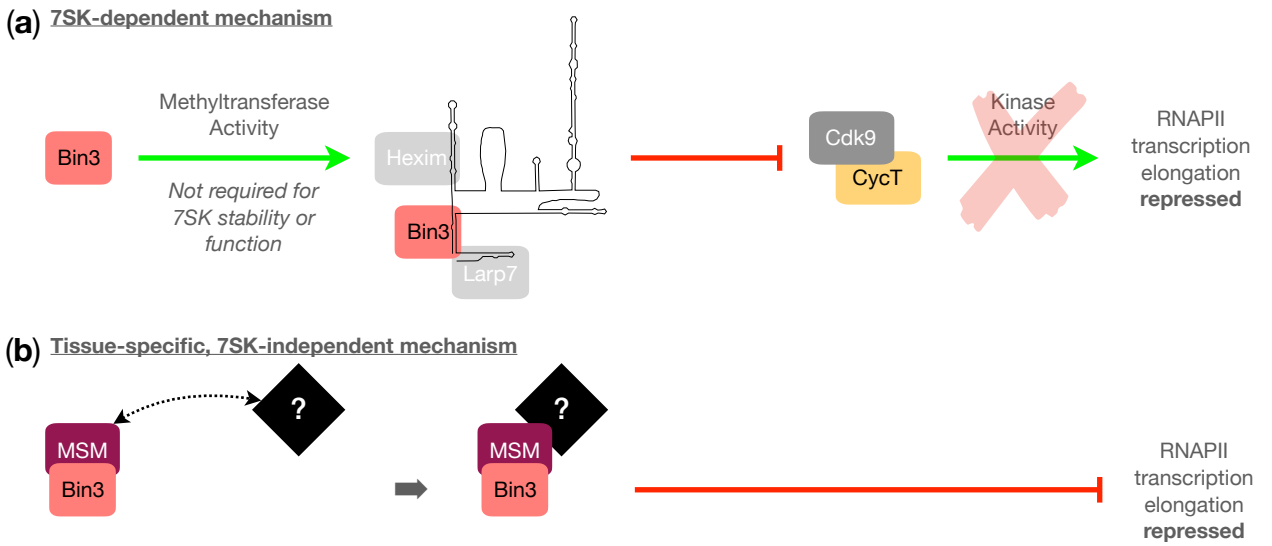
(a) 7SK-dependent mechanism
Bin3
Methyltransferase Activity
Not required for 7SK stability or function
Hexim
Bin3
Larp7
Cdk9
CycT
Kinase Activity
RNAPII transcription elongation repressed
(b) Tissue-specific, 7SK-independent mechanism
?
MSM
Bin3
?
MSM
Bin3
RNAPII transcription elongation repressed